

Planet formation around binary stars: Tatooine made easy

Benjamin C. Bromley

*Department of Physics & Astronomy, University of Utah,
115 S 1400 E, Rm 201, Salt Lake City, UT 84112*

bromley@physics.utah.edu

Scott J. Kenyon

*Smithsonian Astrophysical Observatory,
60 Garden St., Cambridge, MA 02138*

skenyon@cfa.harvard.edu

ABSTRACT

We examine characteristics of circumbinary orbits in the context of current planet formation scenarios. Analytical perturbation theory predicts the existence of nested circumbinary orbits that are generalizations of circular orbits in a Keplerian potential. They contain forced epicyclic motion aligned with the binary as well as higher frequency oscillations, yet they do not cross, even in the presence of massive disks and perturbations from large planets. For this reason, dissipative gas and planetesimals can settle onto these “most circular” orbits, facilitating the growth of protoplanets. Outside a region close to the binary where orbits are generally unstable, circumbinary planets form in much the same way as their cousins around a single star. Here, we review the theory and confirm its predictions with a suite of representative simulations. We then consider the circumbinary planets discovered with NASA’s *Kepler* satellite. These Neptune- and Jupiter-size planets, or their planetesimal precursors, may have migrated inward to reach their observed orbits, since their current positions are outside of unstable zones caused by overlapping resonances. *In situ* formation without migration seems less likely, only because the surface density of the protoplanetary disks must be implausibly high. Otherwise, the circumbinary environment is friendly to planet formation, and we expect that many Earth-like “Tatooines” will join the growing census of circumbinary planets.

Subject headings: planetary systems – planets and satellites: formation – planets and satellites: dynamical evolution and stability – planets and satellites: individual (Kepler-16b, Kepler-34b, Kepler-35b, Kepler-38a, Kepler-47b, PH1, Kepler-413b) – planet disk interactions – stars: binaries

1. Introduction

Planet formation is robust. Transit detections by the *Kepler* satellite (e.g., Borucki et al. 2011; Howard et al. 2012), radial velocity campaigns (Cumming et al. 2008; Howard et al. 2010; Zechmeister et al. 2013; Mayor et al. 2014), direct imaging surveys (Macintosh et al. 2014; Tamura 2014), and gravitational lensing studies (Gould et al. 2010) suggest that many if not all stars host planets (Youdin 2011; Dong & Zhu 2013). To date, there are over 1500 confirmed planets, and several thousand candidates (Han et al. 2014).

The vast majority of the known planets orbit around a single star (e.g., Mayor et al. 2011; Cassan et al. 2012; Burke et al. 2014; Mullally et al. 2015). Their formation in this setting is straightforward to describe, even if certain key details are not well understood (e.g., Safronov 1969; Wetherill 1980; Goldreich et al. 2004; Youdin & Kenyon 2013). The overall process takes many small solid particles of dust and concentrates this mass into a few large objects. Coagulation — growth through sticking or merging of planetesimals — is driven by collisions. Low relative velocities favor growth, but can also slow it down. Higher velocities can speed up the growth rate, but can also lead to destructive collisions. Scattering and gravitational interactions pump up relative velocities, while collisional damping and dynamical friction slow things down. A balance between these processes enables planets to emerge from the dust.

There are a handful of planets known to orbit around binary stars. The first discovered by the Kepler mission is Kepler-16b (Doyle et al. 2011), a Saturn-mass planet at an orbital distance of about 0.7 AU. Its binary host consists of a $0.7 M_{\odot}$ K-type star and a $0.2 M_{\odot}$ red dwarf, at an orbital separation of 0.22 AU. Since then, six more “Tatooines” have been reported in the Kepler data set (see Table 1, below). They are typically Neptune- or Jupiter-size, and all orbit their hosts at distances within roughly 1 AU. One binary, Kepler 47, hosts two such planets (Orosz et al. 2012a). A few more massive circumbinary planets are known or suspected, but these objects orbit at much greater distances compared to the binary semimajor axis (e.g., Beuermann et al. 2011).

The circumbinary planets that orbit close to their hosts provide unique challenges for planet formation. The central stars strongly perturb the region around them, clearing out orbits to distances of 2–5 times the binary separation (Holman & Wiegert 1999). Similarly, circumstellar disks get eroded from the outside by the binary partner. In either case, secular excitations from the binary potential reportedly drive random motions so high that collisions become destructive (Moriwaki & Nakagawa 2004; Meschiari 2012; Paardekooper et al. 2012; Rafikov 2013; Lines et al. 2014). Thus, planets may not be able to grow near their binary host.

To resolve this problem, planets may form at more remote distances, where the time-varying part of the binary potential is weak. To arrive at their observed locations, they must then migrate through the circumbinary gaseous disk or scatter with neighboring gas giants (Pierens & Nelson 2008a,b). While the simulations of this process are compelling (e.g., Kley & Haghighipour 2014), there are uncertainties about starting conditions, typically a set of planetary cores placed into a steady state disk. It is unclear if the simultaneous growth of planetesimals and dissipation of the disk can conspire to produce cores poised to migrate into their observed orbital positions.

Toward understanding how circumbinary planets form, we re-examine a fundamental issue, the nature of planetesimal orbits around binary stars. Following the approach of Lee & Peale (2006) and Leung & Lee (2013), we describe a family of nested, stable circumbinary orbits that have minimal radial excursions and never intersect. While they are not exactly circular, these orbits play the same role as circular paths in a Keplerian potential. Gas and particles can damp to these orbits as they dynamically cool, avoiding the destructive secular excitations reported in previous work. Thus planetesimals may grow *in situ* to full-fledged planets.

We organize this paper to provide an introduction to the Lee-Peal-Leung analytical theory of circumbinary orbits (§2), followed by numerical examples (§3). We then discuss the role these orbits play in planet formation (§4), and close with a comparison to observations (§5), along with a summary and predictions of the ideas presented here (§6).

2. The circumbinary environment

Planet formation relies on the ability of solid particles — dust, planetesimals, protoplanets — to interact gently. Around a single star, the family of nested (concentric) circular orbits offers this possibility. Particles on coplanar circular orbits coexist without any collisions. Gravitational interactions among particles (and with coexisting gas) induce random motions about these circular orbits, which enables particles to merge into larger objects. Unchecked, gravitational interactions grow indefinitely and lead to destructive collisions among particles (e.g., Goldreich & Tremaine 1978). Dynamical cooling (through collisional damping, dynamical friction, or gas drag) is essential (e.g., Goldreich et al. 2004; Youdin & Kenyon 2013). When orbiting particles cool, they need some common set of trajectories on which to settle. The family of circular orbits provides this non-intersecting, collisionless haven for particles in cold circumstellar disks.

A central binary can dramatically alter these orbital dynamics (e.g., Holman & Wiegert

1999; Musielak et al. 2005; Pichardo et al. 2005; Doolin & Blundell 2011). For a primary and secondary with comparable masses and binary eccentricity, e_{bin} , satellite orbits are unstable inside of a critical radius, a_{crit} , which is at least twice the binary separation, a_{bin} . Holman & Wiegert (1999) derive an approximation for a_{crit} from direct simulation of circumbinary particles:

$$a_{\text{crit}} \approx 1.60 + 5.10 e_{\text{bin}} - 2.22 e_{\text{bin}}^2 + 4.12 \frac{M_s}{M_p + M_s} - 4.27 e_{\text{bin}} \frac{M_s}{M_p + M_s} \quad (1)$$

$$-5.09 \frac{M_s^2}{(M_p + M_s)^2} + 4.61 e_{\text{bin}}^2 \frac{M_s^2}{(M_p + M_s)^2}, \quad (2)$$

where M_p and M_s are the masses of the primary and secondary, respectively (see also Pichardo et al. 2005, 2008). Inside this orbital distance, particles are cleared, creating a cavity around the binary.

Particles beyond the critical distance can be on stable, non-Keplerian orbits. In addition to their response to the central mass of the binary, these satellites also experience *forced* motion, driven by the binary’s time-varying potential. This perturbation prevents particles from maintaining a circular orbit. Instead, particles may achieve a “most circular orbit,” defined as having the smallest radial excursion about some guiding center, orbiting at some constant radius R_g and angular speed Ω_g in the plane of the binary (Lee & Peale 2006; Youdin et al. 2012). More generally, circumbinary orbits may be composed of epicyclic motion about R_g , as in the Keplerian case, superimposed on the most circular orbit.

In the rest of this section, we investigate existing analytic theory for circumbinary orbits and applications for planet formation. We also include a brief discussion of instabilities and resonances, as a prelude to numerical simulations in §3.

2.1. Analytical theory of circumbinary orbits

To describe satellite orbits about a central binary, we follow the analytic theories of Lee & Peale (2006) and Leung & Lee (2013). The starting point of these theories is the gravitational potential of the binary:

$$\Phi = -\frac{GM_p}{\sqrt{R^2 + z^2 + R_p^2 + 2RR_p \cos \Delta\phi}} - \frac{GM_s}{\sqrt{R^2 + z^2 + R_s^2 - 2RR_s \cos \Delta\phi}}, \quad (3)$$

where G is the gravitational constant and $\Delta\phi$ is angle between the secondary and the satellite in a reference frame with the binary’s center of mass at the origin. In this frame, the massless satellite is at radial position R in the plane of the binary and has altitude z above this plane. The terms R_p and R_s denote the orbital distances of the primary and secondary.

To make headway, this potential is expanded in terms of the angle cosines, converted from powers ($\cos^k(\Delta\phi)$) to multiple-angle form ($\cos(k\Delta\phi)$). For eccentric binaries, Leung & Lee (2013) also expand the potential to first order in the binary eccentricity, e_{bin} , using the epicyclic approximation to describe the variation in binary separation and phase. Then they seek solutions for the excursion of the satellite from a guiding center on a circular orbit of radius R_g . The excursions in radial, azimuthal and altitude coordinates are δR , $\delta\phi$, and δz (which is identically z , since all vertical motions are excursions from the the guiding center in plane of the binary). Their solution can be estimated by writing the equations of motion and keeping only terms linear in the perturbation coordinates and in the binary eccentricity. Between the expansion of the potential and this linearization, the problem reduces to the form of a simple, driven harmonic oscillator.

In the course of following this prescription, we focus on motion in the binary’s orbital plane. The potential is

$$\Phi \approx \sum_{k=0}^{\infty} \left\{ \Phi_{0k} \cos(k\Delta\phi) + e_{\text{bin}} [\Phi_{0k}^e \cos(k\Delta\phi) \cos(\Omega_{\text{bin}}t) + 2k\Phi_{0k} \sin(k\Delta\phi) \sin(\Omega_{\text{bin}}t)] \right\} \quad [z = 0] \quad (4)$$

where Ω_{bin} is the mean motion of the binary ($\Omega_{\text{bin}}^2 = G(M_p + M_s)/a_{\text{bin}}^3$), and our choice of time t fixes the orbital phases of the binary and satellite. The potentials Φ_{0k} are Fourier coefficients derived from the expansion of the potential in terms of $\cos(\Delta\phi)$ evaluated at $e_{\text{bin}} = 0$, while the Φ_{0k}^e are those same coefficients giving the first-order terms of a Taylor series in e_{bin} . The third set of terms involving the sine functions describes the variation of $\Delta\phi$ with respect to e_{bin} . Examples of these coefficients are

$$\Phi_{00} = -\frac{GM}{R_g} - \frac{G\mu}{R_g} \left[\frac{1}{4} \frac{a_{\text{bin}}^2}{R_g^2} + \frac{9}{64} \frac{(M_p^2 + M_s^2) a_{\text{bin}}^4}{M^2 R_g^4} + \frac{25}{256} \frac{(M_p^4 + M_s^4) a_{\text{bin}}^6}{M^4 R_g^6} + \dots \right] \quad (5)$$

$$\Phi_{01} = -\frac{G\mu}{R_g} \left[\frac{3}{8} \frac{(M_p^2 - M_s^2) a_{\text{bin}}^3}{M^2 R_g^3} + \frac{15}{64} \frac{(M_p^4 - M_s^4) a_{\text{bin}}^5}{M^4 R_g^5} + \dots \right] \quad (6)$$

$$\Phi_{02} = -\frac{G\mu}{R_g} \left[\frac{3}{4} \frac{a_{\text{bin}}^2}{R_g^2} + \frac{5}{16} \frac{(M_p^3 + M_s^3) a_{\text{bin}}^4}{M^3 R_g^4} + \frac{105}{512} \frac{(M_p^5 + M_s^5) a_{\text{bin}}^6}{M^5 R_g^6} + \dots \right] \quad (7)$$

$$\Phi_{03} = -\frac{G\mu}{R_g} \left[\frac{5}{8} \frac{(M_p^2 - M_s^2) a_{\text{bin}}^3}{M^2 R_g^3} + \frac{35}{128} \frac{(M_p^4 - M_s^4) a_{\text{bin}}^5}{M^4 R_g^5} + \dots \right] \quad (8)$$

$$\Phi_{04} = -\frac{G\mu}{R_g} \left[\frac{35}{64} \frac{(M_p^3 + M_s^3) a_{\text{bin}}^4}{M^3 R_g^4} + \frac{63}{256} \frac{(M_p^5 + M_s^5) a_{\text{bin}}^6}{M^5 R_g^6} + \dots \right] \quad (9)$$

$$\Phi_{05} = -\frac{G\mu}{R_g} \left[\frac{63}{128} \frac{(M_p^4 - M_s^4) a_{\text{bin}}^5}{M^4 R_g^5} + \dots \right]; \quad (10)$$

and

$$\Phi_{00}^e = -\frac{G\mu}{R_g} \left[\frac{1}{2} \frac{a_{\text{bin}}^2}{R_g^2} + \frac{9}{16} \frac{M_p^3 + M_s^3}{M^3} \frac{a_{\text{bin}}^4}{R_g^4} + \frac{75}{128} \frac{M_p^5 + M_s^5}{M^5} \frac{a_{\text{bin}}^6}{R_g^6} + \dots \right] \quad (11)$$

$$\Phi_{01}^e = -\frac{G\mu}{R_g} \left[\frac{9}{8} \frac{M_p^2 - M_s^2}{M^2} \frac{a_{\text{bin}}^3}{R_g^3} + \frac{75}{64} \frac{M_p^4 - M_s^4}{M^4} \frac{a_{\text{bin}}^5}{R_g^5} + \dots \right] \quad (12)$$

$$\Phi_{02}^e = -\frac{G\mu}{R_g} \left[\frac{3}{2} \frac{a_{\text{bin}}^2}{R_g^2} + \frac{5}{4} \frac{M_p^3 + M_s^3}{M^3} \frac{a_{\text{bin}}^4}{R_g^4} + \frac{315}{256} \frac{M_p^5 + M_s^5}{M^5} \frac{a_{\text{bin}}^6}{R_g^6} + \dots \right] \quad (13)$$

$$\Phi_{03}^e = -\frac{G\mu}{R_g} \left[\frac{15}{8} \frac{M_p^2 - M_s^2}{M^2} \frac{a_{\text{bin}}^3}{R_g^3} + \frac{175}{128} \frac{M_p^4 - M_s^4}{M^4} \frac{a_{\text{bin}}^5}{R_g^5} + \dots \right] \quad (14)$$

$$\Phi_{04}^e = -\frac{G\mu}{R_g} \left[\frac{35}{16} \frac{M_p^3 + M_s^3}{M^2} \frac{a_{\text{bin}}^4}{R_g^4} + \frac{189}{128} \frac{M_p^5 + M_s^5}{M^4} \frac{a_{\text{bin}}^6}{R_g^6} + \dots \right] \quad (15)$$

$$\Phi_{05}^e = -\frac{G\mu}{R_g} \left[\frac{315}{256} \frac{M_p^4 - M_s^4}{M^4} \frac{a_{\text{bin}}^5}{R_g^5} + \dots \right]. \quad (16)$$

where $M = M_p + M_s$ is the total mass and $\mu = M_p M_s / (M_p + M_s)$ is the reduced mass¹. The subscripts jk designate that each term is measured in the plane of the binary ($j = 0$), and is the k^{th} harmonic as in Equation (3). The missing terms are of order $(a_{\text{bin}}/R_g)^7$, which can be as large as a percent in an idealized system, and a fraction of a percent in observed binaries.

From the time-averaged potential (Φ_{00} in Equation (5)), we can obtain the angular speed of the guiding center, Ω_g . It follows from

$$\Omega_g^2 \equiv \frac{1}{R_g} \left. \frac{d\Phi_{00}}{dR} \right|_{R_g} = \frac{GM}{R_g^3} \left\{ 1 + \frac{\mu}{M} \left[\frac{3}{4} \frac{a_{\text{bin}}^2}{R_g^2} + \frac{45}{64} \frac{(M_p^3 + M_s^3)}{M^3} \frac{a_{\text{bin}}^4}{R_g^4} + \dots \right] \right\}. \quad (17)$$

The square root of Ω_g^2 is the mean motion of the satellite. The satellite's epicyclic and vertical frequencies are

$$\kappa_e^2 \equiv R_g \left. \frac{d\Omega_g^2}{dR} \right|_{R_g} - 4\Omega_g^2 = \frac{GM}{R_g^3} \left\{ 1 - \frac{\mu}{M} \left[\frac{3}{4} \frac{a_{\text{bin}}^2}{R_g^2} + \frac{135}{64} \frac{(M_p^3 + M_s^3)}{M^3} \frac{a_{\text{bin}}^4}{R_g^4} + \dots \right] \right\} \quad (18)$$

$$\nu_i^2 \equiv \frac{1}{z} \left. \frac{d\Phi}{dz} \right|_{z=0, R_g} = \frac{GM}{R_g^3} \left\{ 1 + \frac{\mu}{M} \left[\frac{9}{4} \frac{a_{\text{bin}}^2}{R_g^2} + \frac{225}{64} \frac{(M_p^3 + M_s^3)}{M^3} \frac{a_{\text{bin}}^4}{R_g^4} + \dots \right] \right\} \quad (19)$$

corresponding to the eccentricity and any motion out of the plane of the binary (for details regarding the motion out of the orbital plane, see Lee & Peale 2006). In the limit that the

¹In some previous studies, “ μ ” is defined as the ratio of the secondary’s mass to the total mass. Thus, our μ/M is equal to “ $\mu(1 - \mu)$ ” in Holman & Wiegert (1999), for example.

binary separation goes to zero, or when the binary mass ratio is extreme, both κ_e and ν_i become the Keplerian mean motion.

Forced oscillations experienced by a satellite depend on the synodic frequency,

$$\omega_{\text{syn}} = \Omega_{\text{bin}} - \Omega_{\text{g}}. \quad (20)$$

In general, ω_{syn} is just the average angular speed of the satellite in a reference frame that rotates with the mean motion of the binary. For a circular binary ($e_{\text{bin}} = 0$), the time varying force felt by the satellite depends only on this frequency and its harmonics. In the case of an eccentric binary, the orbital frequency of the binary also enters into the potential.

2.1.1. Equations of motion

Derivatives of the potential yield equations of motion in excursion coordinates $(\delta R, \delta\phi, z)$. The strategy of Lee & Peale (2006) is to cast these equations in the form of a forced harmonic oscillator with natural frequencies κ_e (for δR and $\delta\phi$), ν_i (for the z coordinate) and driving frequencies involving Ω_{bin} and ω_{syn} . The solutions in terms of the full cylindrical coordinates are (Equations (27), (31) and (35) in Leung & Lee 2013):

$$R(t) = R_{\text{g}} \left\{ 1 - e_{\text{free}} \cos(\kappa_e t + \psi_e) - \sum_{k=1}^{\infty} C_k \cos(k\omega_{\text{syn}} t) \right. \quad (21)$$

$$\left. - e_{\text{bin}} \left[C_0^e \cos(\Omega_{\text{bin}} t) + \sum_{k=1}^{\infty} \tilde{C}_k^+ \cos(k\omega_{\text{syn}} t + \Omega_{\text{bin}} t) + \tilde{C}_k^- \cos(k\omega_{\text{syn}} t - \Omega_{\text{bin}} t) \right] \right\}$$

$$\phi(t) = \Omega_{\text{g}} \left\{ t + \frac{2e_{\text{free}}}{\kappa_e} \sin(\kappa_e t + \psi_e) + \sum_{k=1}^{\infty} \frac{D_k}{k\omega_{\text{syn}}} \sin(k\omega_{\text{syn}} t) \right. \quad (22)$$

$$\left. - e_{\text{bin}} \left[\tilde{D}_0^e \cos(\Omega_{\text{bin}} t) + \sum_{k=1}^{\infty} \frac{\tilde{D}_k^+ \cos(k\omega_{\text{syn}} t + \Omega_{\text{bin}} t)}{k\omega_{\text{syn}} + \Omega_{\text{bin}}} + \frac{\tilde{D}_k^- \cos(k\omega_{\text{syn}} t - \Omega_{\text{bin}} t)}{k\omega_{\text{syn}} - \Omega_{\text{bin}}} \right] \right\}$$

$$z(t) = iR_{\text{g}} \cos(\nu_i t + \psi_i), \quad (23)$$

where e_{free} is the “free” eccentricity, i is the inclination, and the phase angles ψ_e and ψ_i are constants. The coefficients are

$$C_k = \frac{1}{R_{\text{g}}} \left. \frac{d\Phi_{0k}}{dR} \right|_{R_{\text{g}}} + \frac{2\Omega_{\text{g}}\Phi_{0k}}{R_{\text{g}}^2\omega_{\text{syn}}} \frac{1}{(\kappa_e^2 - k^2\omega_{\text{syn}}^2)} \quad (24)$$

$$\tilde{C}_0^e = \frac{1}{R_{\text{g}}(\kappa_e^2 - \Omega_{\text{bin}}^2)} \left[\left. \frac{d\Phi_{0k}}{dR} \right]_{R_{\text{g}}} \quad (25)$$

$$\tilde{C}_k^\pm = \frac{1}{R_g [\kappa_e^2 - (k\omega_{\text{syn}} \pm \Omega_{\text{bin}})^2]} \left[\pm k \frac{d\Phi_{0k}}{dR} - \frac{1}{2} \frac{d\Phi_{0k}^e}{dR} - \frac{\pm k\Omega_g (2k\Phi_{0k} \pm \Phi_{0k}^e)}{R(k\omega_{\text{syn}} \pm \Omega_{\text{bin}})} \right]_{R_g} \quad (26)$$

$$D_k = 2C_k - \left[\frac{\Phi_{0k}}{R_g^2 \Omega_g \omega_{\text{syn}}} \right]_{R_g}, \quad (27)$$

$$\tilde{D}_0^e = 2\tilde{C}_k \quad (28)$$

$$\tilde{D}_0^\pm k = 2\tilde{C}_k + \left[\frac{k(\pm 2k\Phi_{0k} - \Phi_{0k}^e)}{2R_g^2 \Omega_g (k\omega_{\text{syn}} \pm \Omega_{\text{bin}})} \right]_{R_g} \quad (29)$$

(Equations (28–30) and (32–34) in Leung & Lee 2013).²

2.1.2. Components of the orbital motion

From the Leung & Lee (2013) solutions, we see that circumbinary orbits may be broken up into independent modes. The first mode is forced motion, prescribed by the characteristics of the binary and the orbital distance of the satellite from the center of mass. The second mode is “free” motion, fully analogous to eccentricity and inclination in a Keplerian system about a single central mass, except that the epicyclic excursions are relative to an orbiting reference frame locked into forced motion, as opposed to a circular guiding center.

The forced motion itself can be broken down into parts, including fast, driven oscillations at the synodic frequency and the binary’s orbital frequency, plus the slower epicyclic oscillations operating at approximately the Keplerian angular frequency. The higher frequency contributions have radial excursion amplitudes that scale as

$$\{C_{02}, \tilde{C}_{02}^\pm\} \times R_g \sim \frac{\mu}{M} \left(\frac{a_{\text{bin}}}{R_g} \right)^5 R_g \quad (30)$$

to leading order in a_{bin}/R_g (e.g., Leung & Lee 2013). The slower epicyclic motion is associated with the forced eccentricity (Heppenheimer 1978). Its contribution to the radial excursions is typically much larger, scaling as

$$e_{\text{force}} R_g = \tilde{C}_{01}^- R_g \approx \frac{5}{4} \frac{M_p - M_s}{M} e_{\text{bin}} a_{\text{bin}}. \quad (31)$$

When the binary eccentricity is large, we can rewrite the the orbit solutions to highlight

²The coefficients \tilde{C} and \tilde{D} are equal to the corresponding C and D in Leung & Lee (2013) divided by the binary eccentricity. For example, $\tilde{C}_k^+ = C_k^+/e_{\text{bin}}$ and $\tilde{C}_0^e = C_0^e/e_{\text{bin}}$. Our choice allows the dependence on binary eccentricity to appear explicitly in the solutions of the excursion variables.

the role of the forced eccentricity. For example, the radial coordinate becomes

$$R(t) = R_g [1 - e_{\text{free}} \cos(\kappa_e t + \psi_e) - e_{\text{force}} \cos(\Omega_g t) + \dots] \quad (32)$$

This form of the solution is familiar from secular perturbation theory (Murray & Dermott 1999).

An important feature of the forced eccentricity is that it does not precess. Its argument of periastron is locked in line with the argument of periastron for the binary’s. All other components of the forced motion are also synchronized to the binary’s orbital frequency, the synodic frequency or their harmonics. In this way, *the orbital paths of satellites experiencing only forced motion make a family of nested orbits that never intersect.*

In contrast to the forced eccentricity, the free eccentricity and inclination are both associated with precession. This effect is a direct result of the fact that even the time-averaged potential around a binary is non-Keplerian — the binary’s mass averaged over its orbit is akin to an oblate spheroid (Heppenheimer 1978; Murray & Dermott 1999; Lee & Peale 2006). The precession rates of the periastron and ascending node are

$$\dot{\omega} = \Omega_g - \kappa_e \approx \frac{3 a_{\text{bin}}^2 \mu}{4 R_g^2 M} \sqrt{GM/R_g^3} \quad (33)$$

$$\dot{\Omega}_{\text{node}} = \Omega_g - \nu_i \approx -\frac{3 a_{\text{bin}}^2 \mu}{4 R_g^2 M} \sqrt{GM/R_g^3} \quad (34)$$

and thus are approximately equal and opposite.

2.1.3. Significance for circumbinary planet formation

The orbit solutions in Equations (21) and (22) have two significant technical features related to how particles orbit in a circumbinary environment:

- The forced epicyclic motion (the \tilde{C}_{01}^- term) is synchronized with the guiding center. If some new, static, axisymmetric potential is added to the binary’s contribution, thus affecting the mean motion (Equation (17)), then the frequency of the forced eccentric motion changes accordingly. The mean motion and epicyclic frequencies remain equal; the satellite remains apsidally aligned with the binary.
- The forced epicyclic motion is coupled in its alignment with the binary. Thus if the binary itself precesses slowly, then the satellite’s argument of periape also precesses. To visualize this point, we note that a slowly precessing binary orbit has slightly different

radial and azimuthal frequencies. To the solutions of Leung & Lee (2013), we thus add the precession rate $\dot{\varpi}_{\text{bin}}$ to the binary’s orbital frequency, Ω_{bin} , without modifying the synodic frequency ω_{syn} between satellite and binary. The terms most greatly affected by this small change are the ones associated with the forced eccentricity (e.g., with \tilde{C}_1^-). The time dependence in these terms then transforms as

$$\cos(\omega_{\text{syn}}t - \Omega_{\text{bin}}t) \rightarrow \cos((\Omega_{\text{g}} + \dot{\varpi}_{\text{bin}})t). \quad (35)$$

Thus the satellite’s forced epicyclic motion precesses with the binary, remaining apsidally aligned (in secular resonance).

These two properties are essential for circumbinary planet formation. They suggest that most circular orbits remain nested and non-intersecting even in the presence of a massive disk or if the binary precesses due to interactions with a massive disk or a distant planetary/stellar perturber (e.g., Rafikov 2013; Silsbee & Rafikov 2015).

2.2. Summary of the analytical theory

The analytic theory of circumbinary orbits predicts a family of nested most circular paths. Satellites orbiting with these paths (i) make well-defined minimal radial excursions and (ii) never collide. Thus, these paths define “dynamically cold” orbits in exactly the same way as circular orbits around single stars. As in the Keplerian case, satellites may have additional “free” eccentricity and inclination to describe motion (perhaps random motion) about these paths. For any combination of free and forced eccentricity, the dynamics of planetesimals as they stir or damp each other takes place in the frame of these most circular paths.

2.3. Limitations of the theory: resonances and chaos

Limitations of the theory stem from its perturbative approach, particularly that it is linear in eccentricities. Aside from singularities in the coefficients in the solutions (e.g., C_{0k} , \tilde{C}_k^\pm) at the 1:1, 1:2 and 1:3 commensurabilities, the theory does not accommodate other resonant effects (cf. Lecar et al. 2001). If the satellite’s epicyclic motion is included as part of the driving force, the solutions may become chaotic and possibly unstable (Wisdom 1980).

The formula for a_{crit} provides a starting point for investigating instability (Equation 1; Holman & Wiegert 1999). In this approximation, the location of unstable orbits close to the

binary varies smoothly with the mass ratio and binary eccentricity. However, locating all of the unstable orbits is more complicated (see also Musielak et al. 2005; Doolin & Blundell 2011). Overlapping resonance conditions generate instability (Wisdom 1980); thus, unstable orbits can exist in narrow, isolated ranges of orbital distance a beyond a_{crit} . In the binary Kepler-16 (Table 1), the 5:1 resonance, located outside of a_{crit} , is unstable. Although it is weaker, the 6:1 resonance is also unstable (e.g., Pierens & Nelson 2007). In between these resonances, orbits are stable; Kepler-16b resides on one of these stable orbits (see Popova & Shevchenko 2013). Beyond the 6:1 resonances, all orbits seem stable. When we discuss formation mechanisms for circumbinary planets, we return to this issue (§5).

3. Numerical simulations

The analytic theory for circumbinary orbits is first-order accurate in the binary eccentricity and is derived from equations of motion linearized in the excursions away from the guiding center. Despite these limitations, it compares well in numerical experiments even when the binary eccentricity is moderately large. We summarize these experiments in this section.

3.1. Code description

We apply our planet formation code ORCHESTRA (Bromley & Kenyon 2006, 2011a) to compare with the theoretical results in §2. ORCHESTRA is a hybrid n -body–coagulation code for tracking the emergence of individual planets (n -bodies) from a sea of smaller particles that can be characterized statistically (the coagulation “grid” with bins for radial position and particle mass). In a standard hybrid calculation, small particles within a set of concentric annuli begin with an adopted radial surface density and initial e and i relative to a circular orbit (see also Safronov 1969; Lissauer 1987; Spaute et al. 1991; Wetherill & Stewart 1993; Weidenschilling 1989; Kenyon & Luu 1998; Kenyon & Bromley 2008). Initially, there are no n -bodies. As massive objects evolve in the grid, the most massive are “promoted” into the n -body part of the code. The subsequent evolution of the n -bodies and the grid are linked together, enabling the simultaneous tracking of gravitational interactions and collisions that lead to accretion, merging and fragmentation (e.g., Kenyon & Bromley 2006, 2010, 2014).

ORCHESTRA has other capabilities which allow us to consider a variety of problems in planet formation and evolution. It can track a swarm of massive or massless tracer particles – usually sampled from orbital distribution of the coagulation particles – to mediate interac-

tions that involve resonances and migration (Bromley & Kenyon 2011b). The code also includes interactions with a massive gas disk, both through gravity (Bromley & Kenyon 2011a) and aerodynamic drag (Weidenschilling 1977a; Kenyon & Bromley 2002). Tests of these and other elements of the code, including our choice of time integrator — either symplectic (Yoshida 1990) or adaptive Richardson extrapolation at 6th-order (Bromley & Kenyon 2006) — are summarized in Kenyon & Bromley (2001), Bromley & Kenyon (2006), Bromley & Kenyon (2011a), and Kenyon & Bromley (2015).

Here we use the n -body component of the code with tracer particles to calculate orbits around a binary. The primary and secondary stars are n -bodies, evolved with the 6th-order symplectic integrator. Energy errors are better than one part in 10^{10} . In some runs (see below) we include a third, Jupiter-mass n -body as a perturber. In others we include the effects of a massive gas disk, choosing a surface density of the form

$$\Sigma_g(a) = \Sigma_{g,0} \frac{a_0}{a}. \quad (36)$$

For a disk similar to the Minimum-Mass Solar Nebula (Weidenschilling 1977b; Hayashi 1981), we adopt $\Sigma_{g,0} = 2000 \text{ g/cm}^2$ and $a_0 = 1 \text{ AU}$. The disk potential is

$$\Phi_d = 2\pi G \Sigma_{g,0} a_0 \log(a/a_0) \quad (37)$$

(Bromley & Kenyon 2011a, Appendix A), from which we derive an acceleration for use in the tracers' equations of motion. This approach allows us to test the analytic theory in §2 using orbit solutions derived numerically at high accuracy.

3.2. Simulation results

Simple n -body experiments with ORCHESTRA allow us to test several key features and predictions of the analytic theory (§2). For these studies, we use the Kepler-16 system as an example (Doyle et al. 2011), adopting binary parameters in Table 1 as estimated by Leung & Lee (2013).

We begin with several illustrations of circumbinary orbits with no other massive perturbers. Our first example focuses on most circular orbits, showing both high-frequency oscillations and epicyclic motion. In a second example, we consider the difference between the time evolution of particles on most circular and ‘initially’ circular orbits around a eccentric binary. Particles on most circular orbits do not precess. Particles which start out on geometrically circular orbits have some free eccentricity; this component of the orbit precesses. By selecting an initially circular orbit with equal parts of free and forced eccentricity, we show how the precession of the free eccentricity modifies trajectories around the binary.

This second example identifies issues with previous n -body studies of circumbinary planet formation (e.g., Moriwaki & Nakagawa 2004; Scholl et al. 2007; Meschiari 2012; Paardekooper et al. 2012). In these analyses, particles with initially geometrically circular orbits precess, developing high relative collision velocities which can inhibit the growth of planetesimals into planets. Most-circular orbits have smaller radial excursions and provide a calmer frame of reference for planet formation.

We then explore the impact of including a massive disk or a Jupiter-mass perturber. Our goal is to determine whether most circular orbits remain “most circular” in the context of a protoplanetary disk around a binary star.

- *A sequence of most circular orbits.* Figure 1 shows the result of test particles on most circular paths near the orbital distance of Kepler-16b. In these orbits, most of the motion comes from the forced eccentricity. As suggested by the Figure, the orbits are all nested and do not intersect.
- *A most circular orbit in detail.* Figure 2 contains radial excursions of a satellite of Kepler-16 in the case where the binary’s eccentricity is reduced by a factor of ten. With this low eccentricity, both the high-frequency driven oscillations and the forced eccentricity are apparent. This Figure shows a direct comparison to theory (Equation (21)).
- *“Circular” versus Most-circular.* Satellites can be launched on paths that are initially more circular (smaller radial excursions) than the most circular orbits discussed here. However, these satellites do not remain on circular paths as their orbits evolve over time. Figure 3 illustrates this point. For a central binary with non-zero e , an orbit with equal parts of free and forced eccentricity can be initialized on a purely circular orbit about the binary center-of-mass. At the start (time = 0 in the figure), this orbit has very little epicyclic motion (e.g., δR is close to zero). Over time, the free eccentricity precesses (Equation (33)); the forced eccentricity does not. Hence the two modes drift in phase, causing the beat pattern in the radial excursion shown in the Figure. Thus, orbits can be geometrically “circular” but only temporarily. Most-circular orbits have the smallest radial excursions over the long term.

Previous studies, including our own (Kenyon & Bromley 2014), describe simulations to track particle dynamics around binaries. If particles are set up initially on geometrically circular orbits (where free and forced eccentricities cancel at $t = 0$), they appear to experience “secular excitations” with the total eccentricity increasing with time until $e = 2e_{\text{force}}$ (Moriwaki & Nakagawa 2004; Scholl et al. 2007; Meschiari 2012; Paardekooper et al. 2012; Rafikov 2013). However, the particles are never actually

stirred by the binary. They simply experience the independent free and forced modes of epicyclic oscillation, acting in concert but not in phase.

- *Most-circular paths around a high-eccentricity binary.* In Figure 4, the eccentricity of the Kepler-16 binary is increased to $e_{\text{bin}} = 0.5$. The satellite is at 0.9 AU, just outside the critical radius for stable orbits for this choice of e_{bin} . The Figure shows samples of the planet’s position in the plane of the binary, taken over the course of 10^4 satellite orbits (blue points in the Figure). The samples reveal the forced eccentricity and demonstrate that the periastron of the satellite is fixed and aligned with the binary. This numerical test is significant: the analytic theory described here is linear, but the n -body experiment is not. The orbital alignment — a prediction of the linear analytic theory — holds in the non-linear case.
- *Orbits in a massive disk.* Figure 4 also demonstrates that most circular orbits do not precess even in the presence of a massive disk. We use a potential as in Equation (36) with a surface density of 2000 g/cm^2 at 1 AU. Around a single star with Kepler-16’s mass, the disk causes rapid apsidal precession of a satellite at 0.9 AU, $\dot{\varpi} \sim 200 \text{ yr}^{-1}$ (Rafikov 2013). However, around the binary, the satellite’s forced eccentricity is immune to precession from the disk, as we expect from perturbation theory. The example in the Figure demonstrates that this prediction extends to moderately large values of the binary’s eccentricity.
- *Effects of stirring: external time-dependent perturbations.* Collisional damping drives particles toward most circular orbits because particles can coexist on these orbits without collisions. Conversely distant massive perturbers (i.e., planets) can gravitationally stir particles, driving them away from most circular paths. From the analytic theory, we expect stirring to behave the same way around a binary as it does around a single star. In Figure 5 we show simulation data from three scenarios: one has a satellite that is like Kepler-16b; another is similar but with a Jupiter mass-body on a circular orbit at 2 AU; and a third has a satellite and a Jupiter, but the binary is replaced by a point mass. The Figure shows that the perturbations of the more distant planet affect the motion of satellites in circumstellar and circumbinary cases in much the same way, by generating nearly identical free eccentricity.
- *Binary precession.* In situations where the binary is eccentric and precessing, our expectation is that the satellite’s forced eccentricity apsidally precess at the same rate. Figure 6 illustrates this effect. We show a precessing binary ($e_{\text{bin}} = 0.5$) in the presence of the same Jupiter-mass perturber as before. In a reference frame rotating with the binary, the satellite’s orbit shows no precession.

3.3. Summary of the numerical studies

To summarize, this set of numerical experiments illustrates that the main predictions of the linear analytic theory are confirmed in the non-linear regime. A key result is that particles initialized on geometrically circular Keplerian orbits have a free eccentricity which precesses, leading to (possibly high velocity) collisions among particles on adjacent orbits. In contrast, most circular orbits remain nested and never cross, even in the presence of a massive disk or a gas giant perturber. Our conclusion is that the standard initial conditions of particles on geometrically circular orbits are not realistic in a dynamically cool planetary disk. The nested most circular orbits are a better starting point. In the next section, we examine these conclusions in the context of planet formation theory.

4. Circumbinary planet formation

In the standard theory of star and planet formation, a rotating molecular cloud of gas and dust collapses into a central protostar and a circumstellar disk (e.g., Cassen & Moosman 1981; Terebey et al. 1984; Yorke et al. 1993). Disk material is on nearly circular orbits (e.g., Weidenschilling 1977a); viscous shear transports mass inward and angular momentum outward (Lynden-Bell & Pringle 1974). Small solids are well-coupled to and flow with the gas (e.g., Adachi et al. 1976; Weidenschilling 1977a; Rafikov 2004). Larger solids decouple from the gas and follow Keplerian orbits about the central star.

Among the decoupled solids, various dynamical processes tend to circularize their orbits around the central star. Smaller particles feel a strong headwind and are dragged towards the central star. Although larger particles feel less drag, the gas efficiently damps their orbits (see also Safronov 1969; Greenberg et al. 1978; Spaute et al. 1991; Wetherill & Stewart 1993). Along with gas drag, collisional damping and dynamical friction drive particles towards circular orbits (e.g., Hornung et al. 1985; Wetherill & Stewart 1993; Kenyon & Luu 1998; Goldreich et al. 2004). As a result, most particles experience small relative collision velocities which encourages growth through mergers (see also Youdin & Kenyon 2013).

When the central protostar is a close binary, we expect a similar evolution. Infalling gas forms a circumbinary disk where the gas and dust generally follow most circular paths around the binary. Aside from an inner gap in the disk roughly at a_{crit} , the structure of the disk orbiting a circular binary is fairly similar to a circumstellar disk around a single star (e.g., Lin & Papaloizou 1979; Pringle 1991; Artymowicz & Lubow 1996). For eccentric binaries, disk material appears to follow most circular orbits with forced eccentricity driven by the central binary (e.g., Pierens & Nelson 2007; Pelupessy & Portegies Zwart 2013). As

long as the disk is not dominated by non-axisymmetric structure (e.g., spiral density waves in a massive disk), we expect pressure and viscosity to induce a smaller inward drift of the gas and small particles relative to most circular orbits (see also Pichardo et al. 2005, 2008). The gas attempts to circularize the orbits of larger particles onto most circular orbits. Collisional damping and dynamical friction also damps the orbits. Thus, large particles end up on most circular orbits with a small amount of free eccentricity with a magnitude similar to the eccentricity of particles in disks around a single star.

Achieving these configurations is a natural long-term outcome for dissipative disks. However, it is worth considering how quickly the gas, dust and larger solid particles can circularize. We can then compare these time scales with time scales for other processes such as precession of the binary. We expect that particles can settle onto most circular orbits when the precession time scales are long compared to circularization time scales. Here, we consider several basic time scales, treating gas-dominated and particle disks as separate cases due to differences in their surface densities and in the physical processes that drive them.

4.1. Gas disks

We start by considering a massive circumbinary disk to model primordial gas in protoplanetary systems (Weidenschilling 1977b; Hayashi 1981). We choose a surface density

$$\Sigma_g(a) = \Sigma_{g,0} \left(\frac{a}{a_0} \right)^{-1} \quad (38)$$

where $\Sigma_{g,0} = 2000 \text{ g/cm}^2$, and $a_0 = 1 \text{ AU}$. The disk has a vertical scale height

$$h(a) = h_{g,0} \left(\frac{a}{a_0} \right)^q \quad (39)$$

where $h_{g,0}/a_0 \sim 0.02$ and $q = 9/7$ (Chiang & Goldreich 1997). Damping times in this disk derive from the sound speed,

$$c_s(a) \sim h(a)v_K/a, \quad (40)$$

where v_K is the orbital velocity at distance a . The damping time is then

$$T_{g,\text{damp}} \sim a/c_s \sim \frac{a^2}{hv_K} \approx 8 \left[\frac{a}{1 \text{ AU}} \right]^{17/14} \left[\frac{M}{1 M_\odot} \right]^{-1/2} \text{ yr.} \quad (41)$$

where M is the total central mass. This time is an upper limit to the time needed for gas to settle on most circular orbits.³

³We are neglecting gas pressure here, but in a static, axisymmetric disk the pressure should act as an additional monopole term in the potential. It would affect the details of the forced motion but would still

By comparison, the time scale for binary precession, a result of the gravitational interaction between the gas disk and the binary, is long. If the inner edge of the disk is at orbital distance a_{in} , then the binary’s apsidal precession rate is (e.g., Ward 1981; Rafikov 2013):

$$\dot{\omega}_{\text{bin}} \approx 0.5 \frac{\pi G \Sigma_g(a_{\text{in}})}{\Omega_{\text{bin}} a_{\text{in}}} \left(\frac{a_{\text{bin}}}{a_{\text{in}}} \right). \quad (42)$$

The precession time is then

$$T_{\text{bin-pre}} \approx 2.0 \times 10^4 \left[\frac{\Sigma_{g,0}}{2000 \text{ g/cm}^2} \right]^{-1} \left[\frac{a_{\text{bin}}}{0.2 \text{ AU}} \right]^{1/2} \left[\frac{a_{\text{in}}}{2.5 a_{\text{bin}}} \right]^3 \text{ yr} \quad [\text{gas disk}], \quad (43)$$

where we choose to set a_{in} to be the innermost stable orbit at $a_{\text{crit}} \approx 2.5 a_{\text{bin}}$, for the values of the parameters in the angular brackets.

Thus the binary precession is slow compared to dynamical times, and the precession is a perturbative effect. We therefore expect that orbits in the disk will remain apsidally aligned with the binary. We conclude that gas disks can damp quickly to most circular orbits, so long as the physics (gravity, hydrodynamics) enables the disk to be axisymmetric (cf. Pelupessy & Portegies Zwart 2013).

4.2. Particle disks

As the gaseous disk evolves, solids particles evolve with it. Small particles remain coupled to the gas. Larger particles with sizes of 1 cm or larger (depending on the local properties of the gas) are uncoupled (e.g., Adachi et al. 1976; Weidenschilling 1977a; Rafikov 2004; Birnstiel et al. 2010). Collisional processes enable some particles to grow to larger sizes (e.g., Windmark et al. 2012; Garaud et al. 2013).

For uncoupled particles, interactions with the gas produce a radial drift and circularize the orbits. The characteristic time scale for these interactions is (Adachi et al. 1976; Weidenschilling 1977a; Rafikov 2004):

$$T_{\text{circ}} \approx 5 \left(\frac{r}{1 \text{ km}} \right) \left(\frac{1 \text{ AU}}{a} \right) \left(\frac{10^{-9} \text{ g cm}^{-3}}{\rho_g} \right) T_{\text{K}}, \quad (44)$$

where r is the radius of the particle, ρ_g is the local gas density (normalized to the typical density of a minimum mass solar nebula), and T_{K} is the orbital period of the local guiding center. For all but very large objects with $r \gtrsim 100 \text{ km}$, this time scale is small compared to

admit solutions that are “most circular”.

the precession time. Thus, small particles uncoupled from the gas likely find most circular orbits.

Numerical simulations of ensembles of small particles interacting with the gas suggest the surface density of the solids is somewhat steeper than the surface density of the gas (e.g., Youdin & Chiang 2004; Brauer et al. 2008; Birnstiel et al. 2010, 2012; Laibe et al. 2012; Pinte & Laibe 2014). Here we adopt a standard power law:

$$\Sigma(a) = \Sigma_0 \left(\frac{a}{a_0} \right)^{-1.5} \quad (45)$$

where $\Sigma_0 = 10 \text{ g/cm}^2$. To derive basic time scales, we assume that particles in the disk have radii of $r = 1 \text{ km}$ and a density of 3 g/cm^3 . If they are stirred to their escape velocity,

$$\begin{aligned} v_{\text{esc}} &= \sqrt{2Gm/r} = \sqrt{8\pi G/3} r \\ &= 0.13 \left[\frac{\rho}{3 \text{ g/cm}^3} \right]^{1/2} \left[\frac{r}{1 \text{ km}} \right] \text{ km/s}, \end{aligned} \quad (46)$$

then we can use standard kinetic theory to estimate the collision time as $(n\sigma v)^{-1}$ where n is the number density, σ is the collisional cross-section, and v is the relative velocity. The damping time from collision is then

$$\begin{aligned} T_{\text{damp}} &\sim \frac{\rho r T_{\text{K}}}{2\sqrt{2}\pi\Sigma} \\ &\approx 3400 \left[\frac{\rho}{3 \text{ g/cm}^3} \right] \left[\frac{r}{1 \text{ km}} \right] \left[\frac{a}{1 \text{ AU}} \right]^6 \left[\frac{\Sigma_0}{10 \text{ g/cm}^2} \right]^{-1} \left[\frac{M}{1 M_{\odot}} \right]^{-1/2} \text{ yr}. \end{aligned} \quad (47)$$

where we have assumed that collisions are inelastic, and that the disk scale height is proportional to the relative speed v , divided by the orbital frequency. This expression ignores gravitational focusing, which reduces the damping time (e.g., Wetherill & Stewart 1993; Ohtsuki 1999).

While the damping time is only linearly dependent on particle size, the range of sizes can be considerable in an evolving planet-forming disk. For pebbles ($r \approx 1 \text{ cm}$), the damping time is very fast: T_{damp} is formally shorter than a dynamical time. For large particles ($\gtrsim 1 \text{ km}$), the time scale for collisional damping is fairly long, approaching the precession time scale for the gas when $r \gtrsim 10 \text{ km}$. However, these larger particles interact with smaller particles through dynamical friction and viscous stirring (e.g., Ohtsuki et al. 2002; Goldreich et al. 2004). For these processes, the typical damping time for large particles is a factor of 10–100 smaller than suggested by Equation (47). Thus, damping times for particles with $r \lesssim 100 \text{ km}$ are short compared to the precession time.

To compare with the binary precession time scale with the inner edge of the particle ring, the precession period is

$$T_{\text{bin-pre}} \approx 4.0 \times 10^6 \left[\frac{\Sigma_0}{10 \text{ g/cm}^2} \right]^{-1} \left[\frac{a_{\text{bin}}}{0.2 \text{ AU}} \right]^{1/2} \left[\frac{a_{\text{in}}}{2.5 a_{\text{bin}}} \right]^3 \text{ yr} \quad [\text{particle disk}]. \quad (48)$$

We conclude that in a particle disk, as in a gas disk, conditions allow for damping to most circular orbits, so they may serve as the equivalent to circular orbits in a Keplerian potential.

Eventually, the largest particles contain more than half the mass of all the solids in an annulus of the disk. At this point, damping times become much longer than stirring times; orbital evolution then becomes chaotic (e.g., Chambers & Wetherill 1998; Goldreich et al. 2004; Kenyon & Bromley 2006). Around a single star, chaotic systems eventually settle down into stable multi-planet systems. Aside from the impact of the inner unstable region and resonances, we expect a similar evolution of chaotic systems around binary stars (e.g., Quintana & Lissauer 2006).

4.3. Perturbations from massive planets

In a particle disk, the binary precession time can be shortened significantly by the presence of a Jupiter-mass planet. If planetesimals orbit within a few times the binary separation and the massive planet orbits well outside this region (e.g., as in Figure 5, $a_{\text{bin}} \sim 0.2 \text{ AU}$, satellite at $a \sim 1 \text{ AU}$ and “jupiter” at 2 AU), then the binary precession rate is

$$\dot{\omega}_{\text{bin}} \approx \frac{3\pi}{4} \frac{m_j}{M} \frac{a_{\text{bin}}^2}{a_j^3}, \quad (49)$$

where M_j and a_j are the planet’s mass and orbital distance. Putting in parameter values that are comparable to observed binary systems and consistent with the set-up in Figure 5, the precession period ($2\pi/\dot{\omega}_{\text{bin}}$) is

$$T_{\text{bin-pre}} \approx 1.2 \times 10^5 \left[\frac{M}{1 M_{\odot}} \right]^{1/2} \left[\frac{M}{1 M_{\text{Jupiter}}} \right]^{-1} \left[\frac{a_{\text{bin}}}{0.2 \text{ AU}} \right]^{-1/2} \left[\frac{a_j}{2 \text{ AU}} \right]^2 \text{ yr}. \quad (50)$$

Any binary precession from the gas giant perturber is a small perturbative effect that preserves the apsidal alignment between binary and planetesimal orbits.

4.4. Planet formation in circumbinary disks

Our analysis establishes time scales for gas and particles to damp to most circular orbits. With no precession of the binary, these orbits do not precess. Although binary precession

induces precession in most circular orbits, these orbits remained apsidally aligned with the binary. In this way, most circular orbits provide reference frames in which the dynamics of planet formation takes place (see also Pichardo et al. 2005, 2008). For example, collisional damping and self-stirring of planetesimals modifies the free eccentricity of circumbinary planetesimals (e.g., as in Wetherill 1980); these processes have no impact on the forced eccentricity (and high-frequency modes) driven by the central binary. Gravitational stirring from distant planets (e.g., Weidenschilling 1989) also excites only the free eccentricity (see Figure 5).

When ensembles of orbiting planetesimals attempt to grow into a planetary system, the relative velocity between particles,

$$v \sim e_{\text{free}} v_{\text{K}}, \quad (51)$$

is a key parameter which establishes the efficiency of gravitational focusing and collision outcomes. Small relative velocities favor growth by mergers; large relative velocities favor destruction. To estimate the boundary between these regimes, we rely on the specific collision energy Q_d^* required to disperse half the mass of a colliding pair of planetesimals to infinity. For rocky material,

$$Q_d^* \approx 3 \times 10^5 \left[\frac{r}{1 \text{ km}} \right]^{-0.4} + 7 \times 10^6 \left[\frac{\rho}{3 \text{ g/cm}^3} \right] \left[\frac{r}{1 \text{ km}} \right]^{1.35} \text{ erg/g} \quad (52)$$

(Davis et al. 1985; Wetherill & Stewart 1993; Benz & Asphaug 1999; Housen & Holsapple 1999; Kenyon & Bromley 2005). Equating Q_d^* to the specific rest-frame collision energy between two equal-mass objects, mass loss exceeds mass gain when

$$v_{\text{dest}} \gtrsim 0.1 \text{ km/s} \quad [\text{destructive collisions, } r = 1 \text{ km}] \quad (53)$$

for kilometer-size rocky planetesimals. This relative speed is best measured in the reference frames of most circular orbits.

Around a binary at orbital distance a , all planetesimals have an additional component to their velocity compared to their counterparts around single stars. This velocity, from the forced eccentricity, has a typical magnitude

$$v \sim v_{\text{force}} \equiv e_{\text{force}} v_{\text{K}} \approx \frac{(M_p - M_s) a_{\text{bin}}}{M} \frac{1}{a} e_{\text{bin}} v_{\text{K}} \quad (54)$$

$$\approx 0.72 \left[\frac{M_p - M_s}{0.5 M_{\odot}} \right] \left[\frac{M}{1 M_{\odot}} \right]^{-1/2} \left[\frac{a_{\text{bin}}}{0.2 \text{ AU}} \right] \left[\frac{e_{\text{bin}}}{0.2} \right] \left[\frac{a}{1 \text{ AU}} \right]^{-3/2} \cdot \text{ km/s} \quad (55)$$

Comparing this value with the disruption speed, it is clear that interpreting v_{force} as a random motion leads to the simple prediction of destructive collisions for a broad range of particle

sizes. Yet v_{force} is the speed of a reference frame tied to a most circular orbit. Particles traveling on most circular orbits have no relative radial velocity; planetesimals may perturb each other and collide, but at velocities much smaller than v_{dest} and v_{force} , promoting mergers instead of destruction.

This picture is different from the approach often taken in previous studies of circumbinary planet formation. For example, in Moriwaki & Nakagawa (2004), Meschiari (2012), Paardekooper et al. (2012), Rafikov (2013), and Lines et al. (2014), particles in n -body simulations are initialized on Keplerian circular orbits about the binary center of mass. From §2 (Equation (21)–(23)), a trajectory with total eccentricity of $e = 0$ is identical to a trajectory with equal parts free and forced eccentricity ($e_{\text{free}} = e_{\text{force}}$), where the phase of the free part is chosen to yield an initial net eccentricity of zero ($\psi_e = \pi$). The difficulty with these initial conditions is that the relative velocities are set with $v \sim e_{\text{free}} v_K \sim v_{\text{force}}$. It is then just a matter of time before precession of the free epicyclic motion drifts from the force motion, and particle orbits can cross. That time is

$$T_{\text{pre}} = \frac{2\pi}{\dot{\varpi}} \approx 67 \left[\frac{a_{\text{bin}}}{0.2 \text{ AU}} \right]^{-2} \left[\frac{a}{1 \text{ AU}} \right]^{7/2} \left[\frac{M}{1 M_{\odot}} \right]^{1/2} \left[\frac{\mu}{0.5 M_{\odot}} \right]^{-1} \text{ yr}, \quad (56)$$

where the reduced mass is $\mu < 0.5M$. Thus, setting up protoplanetary disks with all objects having comparable free and forced eccentricities quickly dooms them to complete destruction.

Sometimes, the initial orbits of circumbinary planetesimals have no impact on the outcome of planet formation calculations. For example, if the free eccentricity is much larger than the forced eccentricity, then the binary’s time varying potential is an unnoticed perturbation. This situation applies in the late stages of planet formation, when most of the mass is concentrated into a small number of large objects. At this stage, large objects have random velocities comparable to the escape velocity of the largest object (e.g., Goldreich et al. 2004; Kenyon & Bromley 2006). Setting $v_{\text{esc}} \gtrsim v_{\text{force}}$, we obtain

$$r_{\text{pro}} \gtrsim 1000 \left[\frac{\rho}{3 \text{ g/cm}^3} \right]^{-1/2} \left[\frac{M}{1 M_{\odot}} \right]^{1/2} \left[\frac{M_p - M_s}{0.5 M_{\odot}} \right] \left[\frac{a_{\text{bin}}}{0.2 \text{ AU}} \right] \left[\frac{e_{\text{bin}}}{0.2} \right] \left[\frac{a}{1 \text{ AU}} \right]^{-3/2} \text{ km}. \quad (57)$$

Outside of the critical radius for stability, a_{crit} , a simulation with a collection of Pluto-size or larger objects should fail to see a difference between circumstellar and circumbinary environments. The simulations of Quintana & Lissauer (2006) support this interpretation. Except for the effects of the destabilization of orbits near a_{crit} , ensembles of roughly lunar mass objects grow into a few terrestrial planets in circumstellar and circumbinary environments.

4.5. Additional issues: resonances and binary evolution

Once planetesimals have settled around most circular paths to grow by coagulation, the binary still influences their evolution. Overlapping resonances may stir particles and destabilize them (Wisdom 1980). However, these unstable orbits are typically close to the binary. For example, the 3:1 resonance, which corresponds to a singularity in the denominator of Equation (25), lies within $2.1a_{\text{bin}}$. As a guide, these unstable orbits are usually within the critical radius a_{crit} identified by Holman & Wiegert (1999). In some binary configurations instabilities extend beyond a_{crit} (e.g., Musielak et al. 2005; Pichardo et al. 2005, 2008; Doolin & Blundell 2011). Numerical simulations provide a straightforward way to identify these orbits (e.g. Popova & Shevchenko 2013) and to understand any impact on gas or solid particles in the planetary disk (e.g., Pierens & Nelson 2008b).

Tidal evolution of the binary can also complicate the long-term stability of circumbinary planetary systems. Changes in the orbital separation and eccentricity can change the positions of critical resonances, leading to instability in systems which had been stable. In Pluto-Charon, systems of satellites become unstable when tidal evolution drives a relatively rapid expansion of the binary orbit (Ward & Canup 2006; Lithwick & Wu 2008; Cheng et al. 2014). For binaries composed of solar-type stars, tidal evolution on time scales of 1–100 Myr is important only for systems with orbital periods of 10 days or less (Meibom & Mathieu 2005). Thus, tidal evolution of the central binary probably has little impact on the formation of most circumbinary planetary systems.

4.6. Summary

Unless the collapse of a molecular cloud into a binary + disk system is significantly different from the collapse to a single star + disk system, we expect the stages of circumbinary planet formation to parallel those of circumstellar planet formation. As long as non-axisymmetric structures such as spiral density waves are relatively unimportant, the time scales for gas damping, gas drag, collisional damping, and dynamical friction are all much shorter than typical precession times for the binary. Thus, material in a circumbinary disk should find its way onto most circular orbits around the binary in a similar way as material in a circumstellar disk damps onto circular orbits around a single star. Once material lies on or close to most circular orbits, small relative velocities of particles on adjacent orbits strongly favors growth over collisional disruption.

Precession of the inner binary has little impact on this conclusion. When a massive disk or giant planet causes the inner binary to precess, the orbits of solid particles on most circular

orbits maintain apsidal alignment. Because relevant time scales for planet formation are much shorter than precession time scales, solids can maintain this apsidal alignment. Most circular orbits remain the reference frame in which to measure relative velocities. Thus, planet formation proceeds in a standard fashion.

For calculations of circumbinary planet formation, starting with the right initial conditions for orbits of gaseous material or solid particles is crucial. Around a single star, it is sufficient to start material on orbits with modest eccentricity: precession is relatively unimportant and all damping processes lead to circular orbits. Around a binary, it is important to differentiate between the forced eccentricity driven by the binary and the free eccentricity relative to a most circular orbit around the binary (see also Pichardo et al. 2005, 2008). Starting particles on circular Keplerian orbits around the binary center of mass creates a free eccentricity relative to a most circular orbit. In general, this free eccentricity is comparable to the forced eccentricity induced by the binary. For eccentric binaries, this extra eccentricity produces spuriously large collision velocities which can lead to collisional destruction instead of growth by merger. To provide a proper evaluation of circumbinary planet formation, it is essential to begin with most circular orbits and then evaluate relative collision velocities for appropriate values of the free eccentricity.

5. Application: The Kepler circumbinary planets

In the last decade, data from the *Kepler* satellite have started to paint a rich picture of circumbinary planetary systems (e.g., Armstrong et al. 2014, and references therein). The known systems (Doyle et al. 2011; Welsh et al. 2012; Orosz et al. 2012a,b; Schwamb et al. 2013; Kostov et al. 2013, 2014) have fairly massive planets with radii $r \approx 0.25\text{--}0.76 R_J$ and semimajor axes $a \approx 0.3\text{--}1.1$ AU orbiting binaries with a broad range of mass ratios (0.25–1) and eccentricities (0.02–0.52). Although the number of circumbinary planetary systems is still rather small (~ 10), detection rates suggest these planets are roughly as common as planets around single stars (Armstrong et al. 2014).

At larger semimajor axes, circumbinary debris disks are also common. Among main sequence stars with FGK spectral types, single stars and binaries are equally likely to have debris disks (Trilling et al. 2007). In circumbinary debris disks, the disk and binary are often co-planar (e.g., Kennedy et al. 2012; Kennedy 2015). Small number statistics currently prevents robust conclusions, but it seems plausible that this structure is primordial: circumbinary disks form in the plane of the binary system (Kennedy et al. 2012; Kennedy 2015).

Understanding the structure of primordial circumbinary disks is also plagued by small numbers (e.g., Harris et al. 2012). Among multiple stars with ages of 1–3 Myr in the Taurus-Auriga molecular cloud, disks around single stars have masses similar to those of very wide binaries with $a \gtrsim 300$ AU. Binaries with $a \approx 30$ –300 AU (5–30 AU) have factor of 3–5 (5–10) smaller disk masses. In four close binaries, however, circumbinary disk masses are comparable in mass to the disks in single stars and wide binaries.

Here, we survey known Kepler circumbinary systems to interpret how their orbital characteristics and size might inform us of their origin. While we reiterate some of the discussion in Leung & Lee (2013), we also focus on how the observations might impact our understanding of planet formation scenarios, whether these planets formed *in situ* or migrated from some larger semimajor axis inward.

To frame the problem, we consider several different formation scenarios:

- I. *In situ formation with no migration.* Planets grow by coagulation from nearby gas and dust. The final planetary mass is limited by the *initial* surface density of the protoplanetary disk. The Minimum-Mass Solar Nebula (MMSN, with $\Sigma_0 = 7$ g/cm² in Equation (36)) provides a useful lower limit on the mass required to build the planets in the solar system. It has $4 M_\oplus$ in solids inside of the snow line a 2.7 AU and roughly $50 M_\oplus$ in solids inside 50 AU (Weidenschilling 1977b; Hayashi 1981). The mass in gas is roughly $800 M_\oplus$ inside 2.7 AU and roughly $3000 M_\oplus$ inside 50 AU. Numerical simulations suggest rocky planet formation is inefficient; collisional processes often lose significant amounts of mass during the assembly of Earth-mass and larger planets (e.g., Kenyon & Bromley 2004, 2006; Raymond et al. 2006, 2011). Augmenting the MMSN by a factor of 2–3 is sufficient to yield Earth-mass planets at 0.7–1 AU in the solar system.

Producing a Neptune-mass planet *in situ* at 1 AU is more challenging. Accreting sufficient gas from the disk to produce Neptune requires a $\sim 10 M_\oplus$ solid core (e.g., Pollack et al. 1996; Rafikov 2011; Rogers et al. 2011; Piso et al. 2015). When the surface density of the disk is roughly 20 times the MMSN, coagulation models routinely produce $10 M_\oplus$ cores (e.g., Hansen & Murray 2012; Schlichting 2014, see below).

In most numerical simulations, formation of 2–3 Earth mass or larger planets is common; producing a single planet is rare (e.g., Kenyon & Bromley 2006; Raymond et al. 2011; Hansen & Murray 2012; Hansen 2014). If these simulations are ‘missing’ an important piece of physics which allows several Earth-mass planets to merge into a single super-Earth mass planet, *in situ* formation of single super-Earth or Neptune mass planets might be possible in lower mass disks, e.g., 3–5 times the mass of the MMSN instead

of ~ 20 times. Without a better understanding, we assume that formation of Neptune mass planets requires a very massive disk.

- II. *Migration then assembly.* Precursor solid material is first moved from large a to within 1 AU of the host star. Planet formation then proceeds *in situ* (Hansen & Murray 2012). In this way, the limited amount of solids available inside of 1 AU is enhanced at early times; the delivery mechanism is uncertain. Because of the structure of the protoplanetary disk at small radii, gas accretion may be less efficient than beyond the snow line. Planets formed in this way may be “gas-starved” compared to more distant gas giants.
- III. *Migration through a gas disk.* Gas giants form beyond the snow line, where the solid-to-gas ratio is a factor of ~ 3 larger (e.g., Lecar et al. 2006). Planets move inward by exchanging torque with the gas disk (Ward 1997). Composition and structure of these planets are typical of the solar system’s gas giants.
- IV. *Planet-planet scattering.* Massive planets formed beyond the snow line gravitationally scatter one another, either inward toward the central mass or outward (Rasio & Ford 1996; Chatterjee et al. 2008; Jurić & Tremaine 2008; Raymond et al. 2010; Marzari et al. 2010; Beaugé & Nesvorný 2012; Moeckel & Armitage 2012; Bromley & Kenyon 2014). In a scattering event between two planets, if the more massive body is Neptune-size or bigger (assuming typical solar system densities and orbital parameters for gas giants), then a broad range of outcomes is possible, including ejection from the system or the placement of a “hot Jupiter” near a single central star. High orbital eccentricity is the red flag for these scattering events.

For each of these modes, the initial mass of the disk and the epoch of planet formation are important considerations (e.g., Najita & Kenyon 2014, and references therein). In the Taurus-Auriga molecular cloud (e.g., Andrews & Williams 2005; Andrews et al. 2013), the median mass in solids for disks around single stars drops from 50–100 M_{\oplus} for protostars (ages of 0.1–0.5 Myr) to 10–20 M_{\oplus} for T Tauri stars (ages of 1–3 Myr). Observations of other star-forming regions suggest this evolution is typical (e.g., Andrews & Williams 2007; Williams & Cieza 2011). Thus, existence of Neptune-mass to Jupiter mass planets favors early formation in the massive disks of young protostars⁴.

⁴For the solar system, radiometric analyses of meteorites similarly suggests formation of solids when the Sun had an age of 0.1–0.3 Myr (e.g., Kleine et al. 2009; Dauphas & Chaussidon 2011).

5.1. Disk mass requirements for *in situ* growth

For *in situ* formation, we estimate the surface density required to make a planet with mass m and radius r . Each protoplanet accretes material from a “feeding zone” with radial width δa . Random motions of particles near the protoplanet set this width. When these particles have random motions smaller than the planet’s escape velocity, the planet can accrete them. For particles with a free eccentricity, $e_{free} \lesssim v_{esc}/v_K$ (e.g., Schlichting 2014). Thus,

$$\Delta a \sim 2ae_{free} \sim 2a\frac{v_{esc}}{v_K} \sim 2a\left(\frac{2am}{rM}\right)^{1/2}. \quad (58)$$

where m and r are the core’s mass and radius⁵. By choosing a form for the surface density (we use $\Sigma \sim a^{-1.5}$ as in Equation (36)) and integrating over the feeding zone (excluding any unstable region inside of a_{crit}) we evaluate the minimum value for Σ at the planet’s position.

Figure 7 shows the results of applying this prescription to the *Kepler* circumbinary planets in Table 1. The minimum surface density required to build gas-accreting cores is roughly an order of magnitude more than the MMSN. Thus, any *in situ* formation model requires a massive disk. Models which form these planets well outside the snow line require much less massive disks.

This result allows us to eliminate *in situ* (no migration) models for all of the *Kepler* circumbinary planets. If the *Kepler* circumbinary planets are common (Armstrong et al. 2014), the precursor disks are also common. Among the youngest stars with ages of 0.1–0.5 Myr, however, disks with initial surface densities of 10–20 times the MMSN are exceedingly rare (Andrews & Williams 2005). Because lower mass protostellar disks are common, the *Kepler* planets require a formation model with some form of migration or scattering.

5.2. Resonances, instabilities and migration

Although formation followed by radial migration is a plausible path for the *Kepler* circumbinary planets, unstable orbital resonances in the circumbinary environment pose clear obstacles to migration (Pierens & Nelson 2007). Near certain commensurabilities, overlapping resonances excite large eccentricities (Lecar et al. 2001). The Holman & Wiegert (1999) condition that orbits are unstable if they are within a distance of a_{crit} from the binary center

⁵This result for the width of the feeding zone is somewhat larger and probably more realistic than the width derived for the more standard “isolation mass” (Greenzweig & Lissauer 1990).

of mass is a working guide; refinements are needed to identify the presence and “strength” of unstable resonances even outside of a_{crit} (e.g., Popova & Shevchenko 2013).

Here, we assess whether the region around each binary in Table 1 is stable as a planet migrates inward. We consider two approaches: directly migrating the planet radially inward and, equivalently, expanding the binary. We show results for binary expansion models, which are more straightforward (and stringent) since they require adjusting only the Keplerian semimajor axis of the binary, instead of modifying the non-Keplerian orbit of the planet to mimic radial drift. Figure 8 shows the results for each *Kepler* planet at an equivalent radial drift rate of less than 10^{-5} AU/yr (typical for planets undergoing type I migration). The particles in the Figure manage to get as close to their binary host as the planet’s current position. Once inside, they become unstable near the 5:1 resonance, except for Kepler-34b, which becomes unstable near the 7:1 commensurability. Kepler-47b, orbiting the binary with the lowest eccentricity, is stable down to the 4:1 resonance. Thus, it seems plausible that the *Kepler* circumbinary planets, or smaller precursors (with fast damping times), could migrate through the potential minefield of resonances. Further tests would need to confirm whether low damping rates or slower migration times would remain stable at the level that we observe.

5.3. The *Kepler* circumbinary planets

With constraints on *in situ* formation and migration from large distances established, we consider whether any of the four modes of planet formation is consistent with the bulk properties and orbit of each *Kepler* circumbinary planet listed in Table 1. We start with the first and most famous discovery, Kepler-16b.

- **Kepler-16.** The central binary, with a K-dwarf primary and an M-dwarf secondary, has significant eccentricity ($e_{\text{bin}} \approx 0.16$). The planet is a gas giant with radius of $0.7 R_J$ and a mass of $0.3 M_J$, orbiting at 0.7 AU with low eccentricity, ~ 0.01 (Doyle et al. 2011). From the analytical theory (§2), Leung & Lee (2013) estimate that free and forced eccentricities are comparable, $e_{\text{free}} \approx e_{\text{force}} \approx 0.03$.

The high mass and low eccentricity of the planet favor the migrate-then-assemble and the migrate-in-gas modes of planet formation. *In situ* formation with no migration, although plausible, requires a very massive disk which is very uncommon among low mass stars with ages of 0.1–0.5 Myr (see Figure 7). Planet-planet scattering is less likely to result in this low-eccentricity configuration (e.g., Marzari et al. 2010; Beaugé & Nesvorný 2012).

- **Kepler-34.** The binary has high eccentricity ($e_{\text{bin}} \approx 0.5$) but the mass difference between the partners is small, within a few percent. Thus, the forced eccentricity at Kepler-34b’s location is low, around 0.002. In contrast, the eccentricity of the planet is much larger, exceeding 0.2. The planet is about the same size as Kepler-16b and may be a Saturn analog. The high eccentricity and high mass favor a scattering scenario.
- **Kepler-35.** This binary has stars that are also nearly equal in mass. The planet, Kepler-35b, is nearly the same size as Kepler-16b and Kepler-34b, but has a much smaller eccentricity (0.048). As with Kepler-16b, the migrate-then-assemble or migrate-in-gas modes are strongly favored over the scattering or *in situ* with no migration formation modes.
- **Kepler-38.** The mass ratio of the binary is almost five to one; the eccentricity is around 0.1. The planet is comparatively small, with a radius of $0.4 R_J$, suggesting a mass of roughly $20 M_{\oplus}$. Despite its low eccentricity (consistent with zero) and low mass, *in situ* formation with no migration is still problematic. Kepler-38b requires a surface density that is more than a factor of twenty larger than the MMSN. The low eccentricity similarly eliminates the scattering mode. Thus, we favor either the migrate-then-assemble or migrate-in-gas mode.
- **Kepler-47.** The binary consists of a Sun-like star and a red dwarf on a nearly circular orbit. The forced eccentricity of its planet is low; the eccentricity of the planet is consistent with zero. With a radius just under $3 R_{\oplus}$, Kepler-47b probably has the smallest mass of all the known circumbinary planets, perhaps $10 M_{\oplus}$. This planet has a companion about twice its radius, Kepler-47c, at an orbital distance of about 1 AU. The combined mass of the two planets works against *in situ* formation with no migration. Two planets orbiting inside the snow line requires a complicated scattering scenario (see Moeckel & Armitage 2012). The migrate-then-assemble and the migrate-in-gas modes are less complicated. Improved statistics for this kind of circumbinary planetary system would provide better constraints on the scattering mode.
- **PH1/Kepler-64.** This binary has both a significant mass difference between its partners and a modestly high eccentricity (0.2). The resulting forced eccentricity is the largest of this sample (0.044). The planet PH1b is half the size of Jupiter, with an eccentricity of 0.05; thus, the free eccentricity is probably low. As with the other Kepler circumbinary planets, the large mass of the planet precludes *in situ* formation with no migration; the small orbital eccentricity eliminates most scattering models. Early formation in a massive disk allows either the migrate-then-assemble or the migrate-in-gas models.

- **Kepler-413.** This low-eccentricity binary hosts a modest size planet, a third the radius of Jupiter. Like Kepler-38b, this mass is uncomfortably high for *in situ* formation without migration. Unlike Kepler-38b, Kepler-413b has a significant free eccentricity of more than 0.1. Large eccentricity tends to preclude the migrate-in-gas mode. However, either the migrate-then-assemble mode or a scattering model can produce a planet similar to Kepler-413b.

5.4. Summary

The circumbinary planets observed by *Kepler* are Neptune-size or bigger and located just beyond the critical radius around their host stars. Although *in situ* planet formation with no migration is a promising way to grow Earth mass planets at these distances, it is very unlikely to be responsible for the known *Kepler* circumbinary planets (Figure 7). The central issue — not enough mass to build Neptune-size planets — is circumvented by importing solids from beyond the snow line. Other formation mechanisms accomplish this mass transfer by invoking an inward radial flux of small particles within the disk, migrating fully-formed gas giants through the disk, or scattering gas giants from outside the snow-line where other large planets form.

Most of the *Kepler* circumbinary planets seem to implicate migration of mass into the region where these objects are observed. Without larger samples of planets, it is impossible to distinguish between models where migration precedes assembly from those where migration follows assembly. All of the planets are too massive to allow *in situ* formation with no migration. However, the high free eccentricity observed in Kepler-34b and Kepler-413b are consistent with scattering events. Improved constraints on the orbits and bulk properties (mass, composition, spin, etc.) might allow more rigorous conclusions on their origin.

Here our most important contribution to the discussion of close-in planets (e.g., Schlichting 2014) is not to firmly discriminate between formation mechanisms, but to emphasize that they are all viable in the circumbinary environment, at least outside of a_{crit} . Thus, the same arguments that take place about the formation of Neptunes inside the snow line may be adopted to the circumbinary case.

6. Discussion

Our main result is that outside of a small region near a binary star, planet formation can proceed in much the same way as around a single star. The reason stems from the existence

of a family of “most circular” orbits around binaries that do not intersect, analogous to concentric circles in a Keplerian potential. Gas, dust and growing planets can orbitally damp to these streamlined paths to avoid mutual collisions. The growth of planets, involving mergers, fragmentation, stirring and dynamical friction, takes place in the reference frame of guiding paths on these most circular orbits, just as it does in circumstellar disks. Without such paths, planetesimal orbits would inevitably mix at high velocity, leading to destruction, not growth.

These most circular paths are rooted in analytical theory. Lee & Peale (2006) and Leung & Lee (2013) lay out the foundation, describing how circumbinary orbits can be approximated as linear combinations of (i) rapid, forced oscillations in response to the time-varying potential, (ii) slower, epicyclic motion — the “forced eccentricity” — that respond to the binary’s eccentricity, and (iii) “free eccentricity” and inclination relative to the plane of the binary. The periapse of the forced eccentricity is aligned with the periapse of the binary. The free eccentricity and inclination have the same meaning for a circumbinary orbit as in a Keplerian system. There is nodal precession of the free eccentricity in the circumbinary case, for the same reason as in the case of a single, oblate star (quadrupole and higher order contributions to the time-averaged gravitational potential).

We place this analytical framework in the context of planet formation. Our results demonstrate that (i) most circular orbits exist for binaries even when their eccentricity is large enough that the theory — based on a perturbative approach — becomes questionable; (ii) non-intersecting, most circular orbits exist in the presence of a massive disk and a large planet; (iii) these orbits remain apsidally aligned with the binary — if the binary precesses, the forced epicyclic paths in the disk also precess; and (iv) the response of a satellite to external perturbations (e.g., stirring from a distant planet) is the same as it would be in a Keplerian potential, in the reference frame of the most circular guiding center. Thus, planets can form *in situ* as close as a few times the orbital separation of their binary hosts. Nearer to home, satellites of the Pluto-Charon binary may have formed in a similar way (Kenyon & Bromley 2014).

To explore whether our results are sensitive to instabilities of circumbinary orbits, we also consider resonant excitations (Artymowicz & Lubow 1994; Kley & Haghighipour 2014). In our tests, the *Kepler* circumbinary planets are all beyond the outermost unstable resonance around their host; for most systems, this is the 5:1 commensurability, close to the prediction of Holman & Wiegert (1999). Our assessment is designed to determine stability over a limited time frame (10^3 – 10^5 yr), not the age of the planetary systems. Nonetheless, they suggest that with typical damping rates and migration times (Papaloizou et al. 2007), both *in situ* formation and migration of planets or their precursors are plausible.

Issues that we do not address include possible non-axisymmetric structure in a massive circumbinary disk (Pelupessy & Portegies Zwart 2013), or the physics near the edge of the stability zone at a distance of a few times the binary separation. Simulations of gas and particle disks can shed light on whether material is pushed outward by torque exchange with the binary or lost in the unstable zone (Artymowicz & Lubow 1996; Günther & Kley 2002). Furthermore, we do not consider tidal evolution of the binary (e.g., Hurley et al. 2002). Depending on the nature of the evolution, variations in binary separation and eccentricity will affect the stability of orbits the circumbinary planetary system. For an intriguing example, see the discussion by Ward & Canup (2006) on resonant transport of moons of around the Pluto-Charon binary as it tidally expands (Bromley & Kenyon 2015).

Our results stand in contrast to previous theoretical studies of circumbinary planet formation. The prevailing view is that dynamical excitation of planetesimals by the binary can lead to destructive collisions (Moriwaki & Nakagawa 2004; Meschiari 2012; Paardekooper et al. 2012; Rafikov 2013; Xie 2013; Lines et al. 2014). In this interpretation, if the binary’s eccentricity is even modestly high, $e_{\text{bin}} \approx 0.2$, epicyclic velocities eventually exceed the shattering speed for all but the biggest planetesimals over a significant range of orbital distances. In this view, planet formation close to the binary is impossible.

These conclusions depend on the assumption that planetesimals initially are on orbits with no eccentricity in the Keplerian sense (see Figure 1 in Lines et al. 2014). In light of analytical theory (§2), this choice endows particles with equal amounts of free and forced eccentricity. As the free part drifts in phase, collisions may destroy growing protoplanets. A more realistic approach to modeling an unstirred disk is to set the planetesimals on most circular orbits with no free eccentricity. Absent any stirring, these bodies orbit an eccentric binary host indefinitely without colliding. If planetesimals develop small random motions about the most circular orbits, collision velocities are modest, just as for planetesimals with modest random motions about a circular orbit around a single star. Modest collision velocities promote growth instead of destruction. Planet formation close to the binary is then robust.

Finally, we review characteristics of *Kepler* circumbinary planets in light of our results. If circumbinary planets form roughly *in situ*, the orbital characteristics and sizes of these planets require very large initial surface densities (10–20 times the MMSN). Although these high surface densities appear to preclude *in situ* models with no migration, the migrate-then-assemble picture of Hansen & Murray (2012) is viable. As a plausible alternative, migrate-in-gas models allow these planets to form beyond the snow line and migrate inward through the gas. For this set of Kepler planets, migration through gas can avoid unstable resonances around the binary. For Kepler-34b and Kepler-413b, formation beyond the snow

line followed by a scattering event is also a reasonable scenario.

In general, the evolution of solids on most circular orbits around a binary differs little from the evolution of solids on circular orbits around a single star. Thus, the standard issues of formation around single stars (e.g., migration, resonances, scattering, etc) have clear parallels in circumbinary disks (for a summary of the issues in single stars, see Schlichting 2014). In light of our results, all options available to circumstellar disks are also available to circumbinary disks.

We conclude with predictions for circumbinary planetary systems. In our scenario, planets are as prevalent around binaries as around single stars. Furthermore, relative to coplanar, most circular orbits, these planets should have the same distribution of orbital elements (free eccentricity and inclination) as their circumstellar cousins. Data from the full Kepler catalog indeed suggest that the planets have comparable rates around binaries and single stars (Armstrong et al. 2014). Tatooine sunsets may be common after all.

We gratefully acknowledge NASA for support through the Outer Planets Program (grant NNX11AM37G) and for a generous allocation of time on the 'discover' supercomputing cluster. This research has made use of the Exoplanet Orbit Database and the Exoplanet Data Explorer at exoplanets.org.

REFERENCES

- Adachi, I., Hayashi, C., & Nakazawa, K. 1976, *Progress of Theoretical Physics*, 56, 1756
- Andrews, S. M., Rosenfeld, K. A., Kraus, A. L., & Wilner, D. J. 2013, *ApJ*, 771, 129
- Andrews, S. M., & Williams, J. P. 2005, *ApJ*, 631, 1134
- . 2007, *ApJ*, 671, 1800
- Armstrong, D. J., Osborn, H. P., Brown, D. J. A., et al. 2014, *MNRAS*, 444, 1873
- Artymowicz, P., & Lubow, S. H. 1994, *ApJ*, 421, 651
- . 1996, *ApJ*, 467, L77
- Beaugé, C., & Nesvorný, D. 2012, *ApJ*, 751, 119
- Benz, W., & Asphaug, E. 1999, *Icarus*, 142, 5

- Beuermann, K., Buhlmann, J., Diese, J., et al. 2011, *A&A*, 526, A53
- Birnstiel, T., Andrews, S. M., & Ercolano, B. 2012, *A&A*, 544, A79
- Birnstiel, T., Dullemond, C. P., & Brauer, F. 2010, *A&A*, 513, A79+
- Borucki, W. J., Koch, D. G., Basri, G., et al. 2011, *ApJ*, 736, 19
- Brauer, F., Dullemond, C. P., & Henning, T. 2008, *A&A*, 480, 859
- Bromley, B. C., & Kenyon, S. J. 2006, *AJ*, 131, 2737
- . 2011a, *ApJ*, 731, 101
- . 2011b, *ApJ*, 735, 29
- . 2014, *ApJ*, 796, 141
- . 2015, in preparation.
- Burke, C. J., Bryson, S. T., Mullally, F., et al. 2014, *ApJS*, 210, 19
- Cassan, A., Kubas, D., Beaulieu, J.-P., et al. 2012, *Nature*, 481, 167
- Cassen, P., & Moosman, A. 1981, *Icarus*, 48, 353
- Chambers, J. E., & Wetherill, G. W. 1998, *Icarus*, 136, 304
- Chatterjee, S., Ford, E. B., Matsumura, S., & Rasio, F. A. 2008, *ApJ*, 686, 580
- Cheng, W. H., Peale, S. J., & Lee, M. H. 2014, *Icarus*, 241, 180
- Chiang, E. I., & Goldreich, P. 1997, *ApJ*, 490, 368
- Cumming, A., Butler, R. P., Marcy, G. W., et al. 2008, *PASP*, 120, 531
- Dauphas, N., & Chaussidon, M. 2011, *Annual Review of Earth and Planetary Sciences*, 39, 351
- Davis, D. R., Chapman, C. R., Weidenschilling, S. J., & Greenberg, R. 1985, *Icarus*, 63, 30
- Dong, S., & Zhu, Z. 2013, *ApJ*, 778, 53
- Doolin, S., & Blundell, K. M. 2011, *MNRAS*, 418, 2656
- Doyle, L. R., Carter, J. A., Fabrycky, D. C., et al. 2011, *Science*, 333, 1602

- Garaud, P., Meru, F., Galvagni, M., & Olczak, C. 2013, *ApJ*, 764, 146
- Goldreich, P., Lithwick, Y., & Sari, R. 2004, *ARA&A*, 42, 549
- Goldreich, P., & Tremaine, S. D. 1978, *Icarus*, 34, 227
- Gould, A., Dong, S., Gaudi, B. S., et al. 2010, *ApJ*, 720, 1073
- Greenberg, R., Hartmann, W. K., Chapman, C. R., & Wacker, J. F. 1978, *Icarus*, 35, 1
- Greenzweig, Y., & Lissauer, J. J. 1990, *Icarus*, 87, 40
- Günther, R., & Kley, W. 2002, *A&A*, 387, 550
- Han, E., Wang, S. X., Wright, J. T., et al. 2014, *PASP*, 126, 827
- Hansen, B. M. S. 2014, *ArXiv e-prints*, arXiv:1403.6553
- Hansen, B. M. S., & Murray, N. 2012, *ApJ*, 751, 158
- Harris, R. J., Andrews, S. M., Wilner, D. J., & Kraus, A. L. 2012, *ApJ*, 751, 115
- Hayashi, C. 1981, *Progress of Theoretical Physics Supplement*, 70, 35
- Heppenheimer, T. A. 1978, *A&A*, 65, 421
- Holman, M. J., & Wiegert, P. A. 1999, *AJ*, 117, 621
- Hornung, P., Pellat, R., & Barge, P. 1985, *Icarus*, 64, 295
- Housen, K. R., & Holsapple, K. A. 1999, *Icarus*, 142, 21
- Howard, A. W., Marcy, G. W., Johnson, J. A., et al. 2010, *Science*, 330, 653
- Howard, A. W., Marcy, G. W., Bryson, S. T., et al. 2012, *ApJS*, 201, 15
- Hurley, J. R., Tout, C. A., & Pols, O. R. 2002, *MNRAS*, 329, 897
- Jurić, M., & Tremaine, S. 2008, *ApJ*, 686, 603
- Kennedy, G. M. 2015, *MNRAS*, 447, L75
- Kennedy, G. M., Wyatt, M. C., Sibthorpe, B., et al. 2012, *MNRAS*, 426, 2115
- Kenyon, S. J., & Bromley, B. C. 2001, *AJ*, 121, 538
- . 2002, *AJ*, 123, 1757

- . 2004, *ApJ*, 602, L133
- . 2005, *AJ*, 130, 269
- . 2006, *AJ*, 131, 1837
- . 2008, *ApJS*, 179, 451
- . 2010, *ApJS*, 188, 242
- . 2014, *AJ*, 147, 8
- . 2015, ArXiv e-prints, arXiv:1501.05659
- Kenyon, S. J., & Luu, J. X. 1998, *AJ*, 115, 2136
- Kleine, T., Touboul, M., Bourdon, B., et al. 2009, *Geochim. Cosmochim. Acta*, 73, 5150
- Kley, W., & Haghighipour, N. 2014, *A&A*, 564, A72
- Kostov, V. B., McCullough, P. R., Hinse, T. C., et al. 2013, *ApJ*, 770, 52
- Kostov, V. B., McCullough, P. R., Carter, J. A., et al. 2014, *ApJ*, 784, 14
- Laibe, G., Gonzalez, J.-F., & Maddison, S. T. 2012, *A&A*, 537, A61
- Lecar, M., Franklin, F. A., Holman, M. J., & Murray, N. J. 2001, *ARA&A*, 39, 581
- Lecar, M., Podolak, M., Sasselov, D., & Chiang, E. 2006, *ApJ*, 640, 1115
- Lee, M. H., & Peale, S. J. 2006, *Icarus*, 184, 573
- Leung, G. C. K., & Lee, M. H. 2013, *ApJ*, 763, 107
- Lin, D. N. C., & Papaloizou, J. 1979, *MNRAS*, 188, 191
- Lines, S., Leinhardt, Z. M., Paardekooper, S., Baruteau, C., & Thebault, P. 2014, *ApJ*, 782, L11
- Lissauer, J. J. 1987, *Icarus*, 69, 249
- Lithwick, Y., & Wu, Y. 2008, ArXiv e-prints, arXiv:0802.2939
- Lynden-Bell, D., & Pringle, J. E. 1974, *MNRAS*, 168, 603
- Macintosh, B., Graham, J. R., Ingraham, P., et al. 2014, ArXiv e-prints, arXiv:1403.7520

- Marzari, F., Baruteau, C., & Scholl, H. 2010, *A&A*, 514, L4
- Mayor, M., Lovis, C., & Santos, N. C. 2014, *Nature*, 513, 328
- Mayor, M., Marmier, M., Lovis, C., et al. 2011, ArXiv e-prints, arXiv:1109.2497
- Meibom, S., & Mathieu, R. D. 2005, *ApJ*, 620, 970
- Meschiari, S. 2012, *ApJ*, 752, 71
- Moeckel, N., & Armitage, P. J. 2012, *MNRAS*, 419, 366
- Moriwaki, K., & Nakagawa, Y. 2004, *ApJ*, 609, 1065
- Mullally, F., Coughlin, J. L., Thompson, S. E., et al. 2015, ArXiv e-prints, arXiv:1502.02038
- Murray, C. D., & Dermott, S. F. 1999, *Solar system dynamics* (Princeton: Princeton University Press)
- Musielak, Z. E., Cuntz, M., Marshall, E. A., & Stuit, T. D. 2005, *A&A*, 434, 355
- Najita, J. R., & Kenyon, S. J. 2014, *MNRAS*, 445, 3315
- Ohtsuki, K. 1999, *Icarus*, 137, 152
- Ohtsuki, K., Stewart, G. R., & Ida, S. 2002, *Icarus*, 155, 436
- Orosz, J. A., Welsh, W. F., Carter, J. A., et al. 2012a, *Science*, 337, 1511
- . 2012b, *ApJ*, 758, 87
- Paardekooper, S.-J., Leinhardt, Z. M., Thébault, P., & Baruteau, C. 2012, *ApJ*, 754, L16
- Papaloizou, J. C. B., Nelson, R. P., Kley, W., Masset, F. S., & Artymowicz, P. 2007, *Protostars and Planets V*, 655
- Pelupessy, F. I., & Portegies Zwart, S. 2013, *MNRAS*, 429, 895
- Pichardo, B., Sparke, L. S., & Aguilar, L. A. 2005, *MNRAS*, 359, 521
- . 2008, *MNRAS*, 391, 815
- Pierens, A., & Nelson, R. P. 2007, *A&A*, 472, 993
- . 2008a, *A&A*, 478, 939
- . 2008b, *A&A*, 483, 633

- Pinte, C., & Laibe, G. 2014, *A&A*, 565, A129
- Piso, A.-M. A., Youdin, A. N., & Murray-Clay, R. A. 2015, *ApJ*, 800, 82
- Pollack, J. B., Hubickyj, O., Bodenheimer, P., et al. 1996, *Icarus*, 124, 62
- Popova, E. A., & Shevchenko, I. I. 2013, *ApJ*, 769, 152
- Pringle, J. E. 1991, *MNRAS*, 248, 754
- Quintana, E. V., & Lissauer, J. J. 2006, *Icarus*, 185, 1
- Rafikov, R. R. 2004, *AJ*, 128, 1348
- . 2011, *ApJ*, 727, 86
- . 2013, *ApJ*, 764, L16
- Rasio, F. A., & Ford, E. B. 1996, *Science*, 274, 954
- Raymond, S. N., Armitage, P. J., & Gorelick, N. 2010, *ApJ*, 711, 772
- Raymond, S. N., Quinn, T., & Lunine, J. I. 2006, *Icarus*, 183, 265
- Raymond, S. N., Armitage, P. J., Moro-Martín, A., et al. 2011, *A&A*, 530, A62
- Rogers, L. A., Bodenheimer, P., Lissauer, J. J., & Seager, S. 2011, *ApJ*, 738, 59
- Safronov, V. S. 1969, *Evoliutsiia doplanetnogo oblaka. (Evolution of the Protoplanetary Cloud and Formation of the Earth and Planets, Nauka, Moscow [Translation 1972, NASA TT F-677] (1969.)*
- Schlichting, H. E. 2014, *ApJ*, 795, L15
- Scholl, H., Marzari, F., & Thébault, P. 2007, *MNRAS*, 380, 1119
- Schwamb, M. E., Orosz, J. A., Carter, J. A., et al. 2013, *ApJ*, 768, 127
- Silsbee, K., & Rafikov, R. R. 2015, *ApJ*, 798, 71
- Spaute, D., Weidenschilling, S. J., Davis, D. R., & Marzari, F. 1991, *Icarus*, 92, 147
- Tamura, M. 2014, in *American Astronomical Society Meeting Abstracts, Vol. 224, American Astronomical Society Meeting Abstracts 224*, 301.03
- Terebey, S., Shu, F. H., & Cassen, P. 1984, *ApJ*, 286, 529

- Trilling, D. E., Stansberry, J. A., Stapelfeldt, K. R., et al. 2007, *ApJ*, 658, 1289
- Ward, W. R. 1981, *Icarus*, 47, 234
- . 1997, *Icarus*, 126, 261
- Ward, W. R., & Canup, R. M. 2006, *Science*, 313, 1107
- Weidenschilling, S. J. 1977a, *MNRAS*, 180, 57
- . 1977b, *Ap&SS*, 51, 153
- . 1989, *Icarus*, 80, 179
- Welsh, W. F., Orosz, J. A., Carter, J. A., et al. 2012, *Nature*, 481, 475
- Wetherill, G. W. 1980, *ARA&A*, 18, 77
- Wetherill, G. W., & Stewart, G. R. 1993, *Icarus*, 106, 190
- Williams, J. P., & Cieza, L. A. 2011, *ARA&A*, 49, 67
- Windmark, F., Birnstiel, T., Ormel, C. W., & Dullemond, C. P. 2012, *A&A*, 544, L16
- Wisdom, J. 1980, *AJ*, 85, 1122
- Xie, J. W. 2013, *Acta Astronomica Sinica*, 54, 79
- Yorke, H. W., Bodenheimer, P., & Laughlin, G. 1993, *ApJ*, 411, 274
- Yoshida, H. 1990, *Physics Letters A*, 150, 262
- Youdin, A. N. 2011, *ApJ*, 742, 38
- Youdin, A. N., & Chiang, E. I. 2004, *ApJ*, 601, 1109
- Youdin, A. N., & Kenyon, S. J. 2013, in *Planets, Stars and Stellar Systems. Volume 3: Solar and Stellar Planetary Systems*, ed. T. D. Oswalt, L. M. French, & P. Kalas (Dordrecht: Springer Science & Business Media), 1
- Youdin, A. N., Kratter, K. M., & Kenyon, S. J. 2012, *ArXiv e-prints*, arXiv:1205.5273
- Zechmeister, M., Kürster, M., Endl, M., et al. 2013, *A&A*, 552, A78

Table 1: Kepler binaries. Along with orbital parameters are estimates of the innermost stable orbit radius (a_{crit}) and the forced eccentricity (e_{force}).

| | $M_p (M_\odot)$ | $M_s (M_\odot)$ | $a_{\text{bin}} (\text{AU})$ | e_{bin} | $a (\text{AU})$ | e | $r (\text{R}_J)$ | $a_{\text{crit}} (\text{AU})$ | e_{force} |
|-------------------------|-----------------|-----------------|------------------------------|------------------|-----------------|--------|------------------|-------------------------------|--------------------|
| Kepler-16 ^a | 0.687 | 0.202 | 0.224 | 0.160 | 0.720 | 0.024 | 0.75 | 0.646 | 0.034 |
| Kepler-34 ^a | 1.049 | 1.022 | 0.228 | 0.521 | 1.086 | 0.209 | 0.76 | 0.833 | 0.002 |
| Kepler-35 ^a | 0.885 | 0.808 | 0.176 | 0.142 | 0.605 | 0.048 | 0.73 | 0.496 | 0.002 |
| Kepler-38 ^b | 0.949 | 0.249 | 0.147 | 0.103 | 0.464 | <0.032 | 0.39 | 0.389 | 0.024 |
| Kepler-47 ^c | 1.043 | 0.362 | 0.084 | 0.023 | 0.296 | <0.035 | 0.27 | 0.203 | 0.004 |
| PH1 ^d | 1.528 | 0.378 | 0.174 | 0.212 | 0.634 | 0.054 | 0.55 | 0.527 | 0.044 |
| Kepler-413 ^e | 0.820 | 0.542 | 0.099 | 0.037 | 0.355 | 0.118 | 0.39 | 0.253 | 0.003 |

^aSee Doyle et al. (2011) and Welsh et al. (2012); orbital elements are from Leung & Lee (2013, Table 1);

^bOrosz et al. (2012b).

^cOrosz et al. (2012a); A second planet ($r = 0.41 \text{ R}_J$) is at $\sim 1 \text{ AU}$.

^dSchwamb et al. (2013) and Kostov et al. (2013); Kepler-64.

^eKostov et al. (2014).

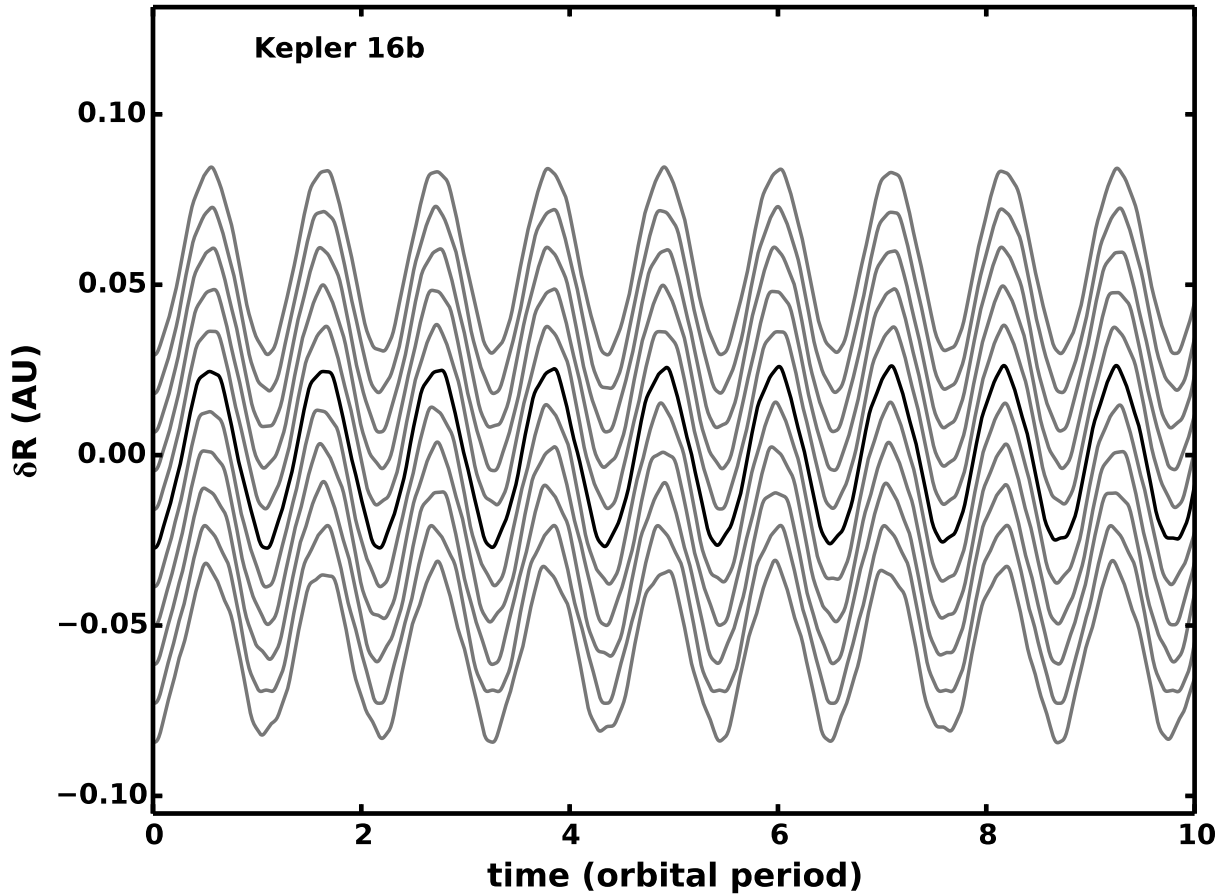


Fig. 1.— The radial excursion of Kepler-16b on most circular orbits. The dark curve shows the radial excursion of a satellite at the orbital position of the planet in the absence of free eccentricity and inclination, plotted as a function of orbital phase (in units of the planet’s orbital period). The light curves show orbits at slightly displaced orbital distances. The trajectories are dominated by the forced eccentricity. Comparatively small higher-frequency oscillations are visible in the curves. Despite the appearance that these oscillations are not in phase between the curves, the orbits do not cross.

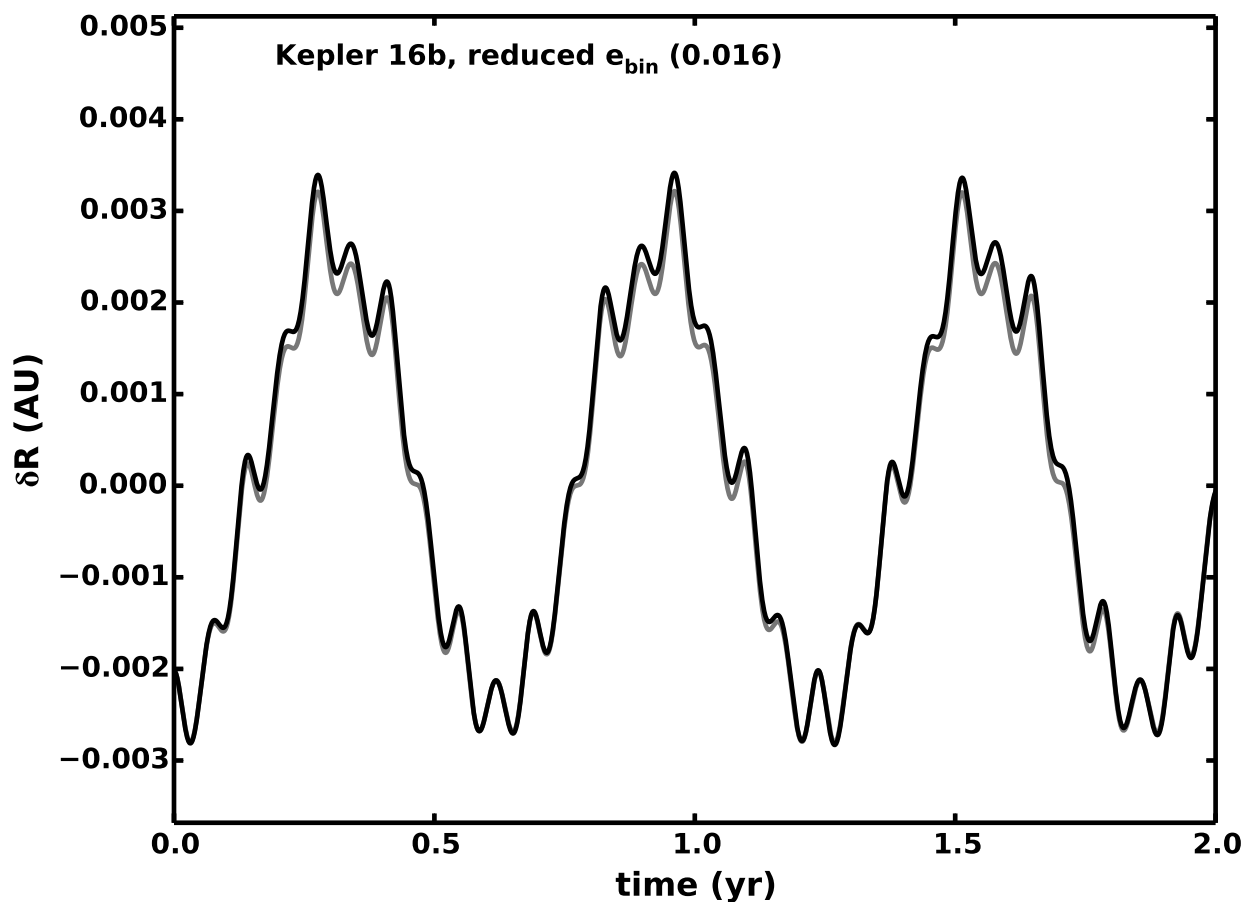


Fig. 2.— Illustration of radial excursions of a satellite on a most circular orbit. The orbital configuration and binary masses are derived from Kepler-16 and its planet Kepler-16b at $a = 0.70$ AU. The binary eccentricity has been reduced by a factor of 10 from the real system; the plot then distinguishes the forced eccentricity (larger amplitude, driven at the orbital period, ~ 0.6 yr) and the high-frequency oscillations (smaller amplitude driven at the binary’s orbital period and the synodic period of the satellite relative to the binary, ~ 0.1 yr). The dark curve is from simulation while the light curve is from analytical theory (Equation (21)).

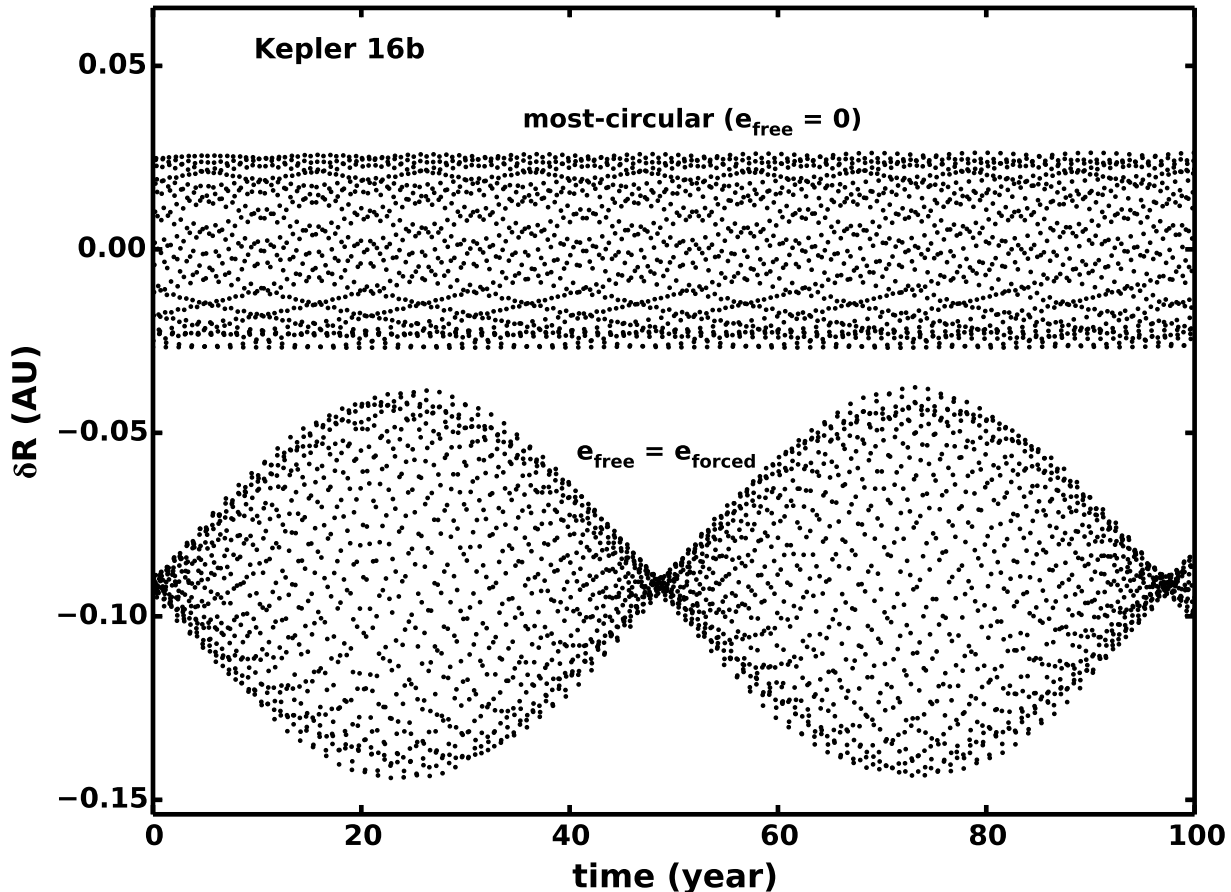


Fig. 3.— Comparison between a most circular orbit and one initially on the circular path of the guiding center (zero eccentricity). The most circular path (upper curve) is non-precessing, with excursions from the guiding center that have a maximum amplitude that does not drift over time. In contrast, a particle that is set up on a “circular” orbit — launching the particle from its guiding center with the speed of uniform circular motion about the binary center of mass — has a mixture of free and force eccentricities in equal measure. The relative phase allows zero eccentricity at the start. The result (lower curve, displaced from the upper one for clarity) is the beat pattern with a frequency given by the nodal precession rate of the free eccentricity (Equation (33)).

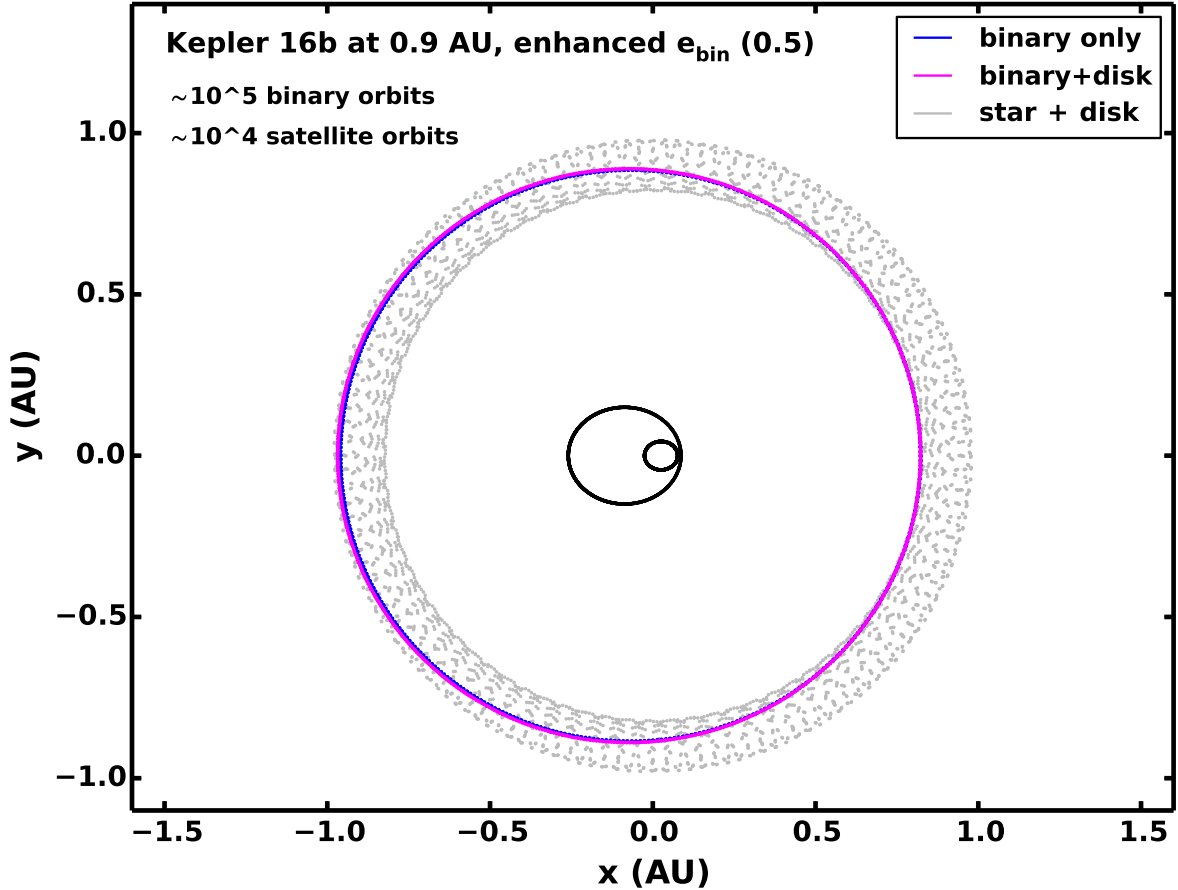


Fig. 4.— Simulated most circular orbits around a binary with moderately high eccentricity. The orbital configuration is derived from Kepler-16, as in the previous figures, but the binary eccentricity is set to 0.5, and the satellite is placed at 0.9 AU, just beyond the critical radius for stability ($a_{\text{crit}} = 0.86$ AU). The center of mass of the system is at the origin in this $x - y$ map of the plane of the binary. The secondary’s pericenter is on the positive x -axis. The satellite (blue dots) tracks a narrow elliptical path with an eccentricity of $e_{\text{force}} \approx 0.08$, fixed and aligned with the binary for $\sim 10^4$ orbital periods ($\sim 10^5$ binary orbits). When the potential of a massive disk (Σ of 2000 g/cm^2 at 1 AU) is included, the satellite’s most circular path does not precess (magenta points, mixed in with the blue ones). For reference, we show samples of a satellite orbiting a single star with Kepler-16’s total mass, also in this disk potential (grey points). In this case, the precession of the satellite’s argument of periastron is rapid ($\sim 200 \text{ rad/yr}$); the points fill an annular swath. In these simulations, there is no interaction between the disk and the binary.

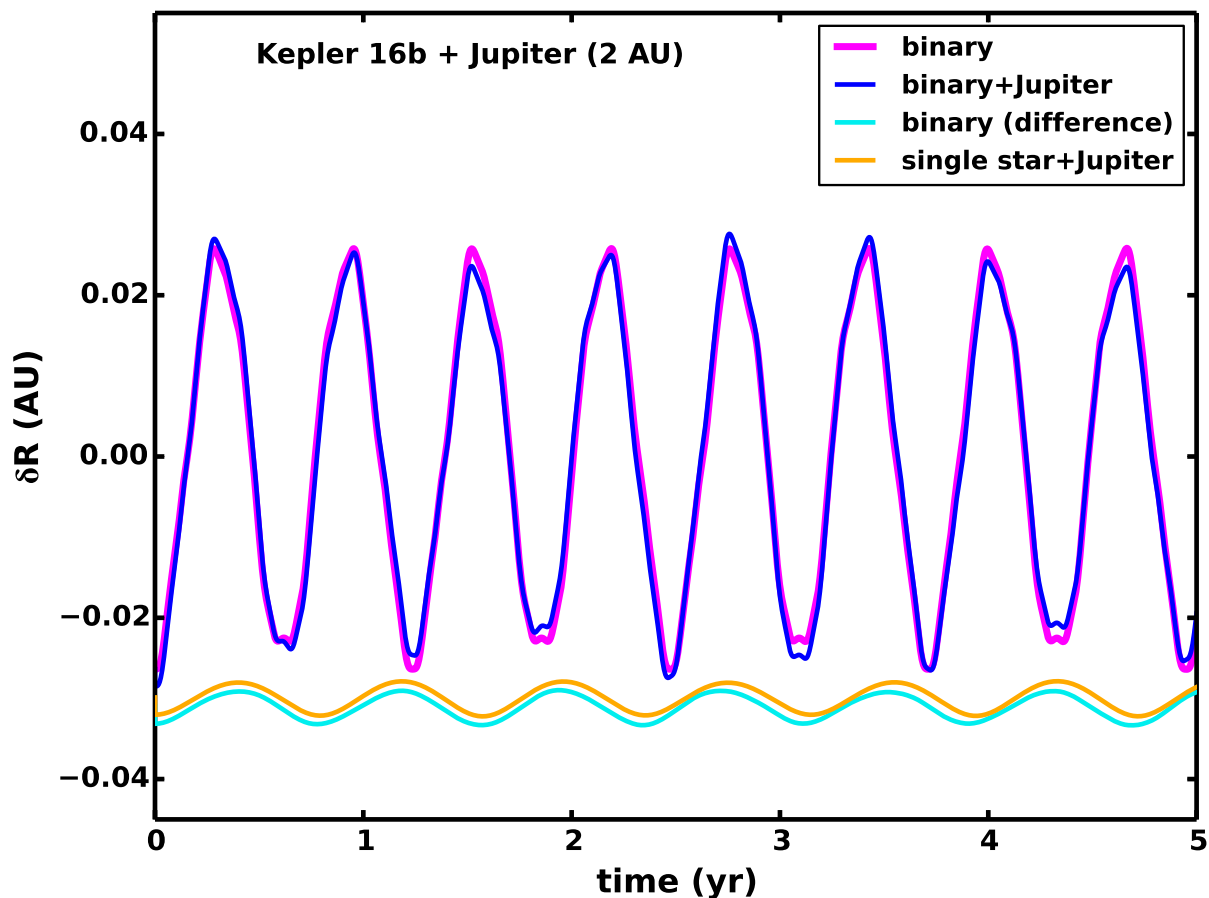


Fig. 5.— The effect of an external perturber on circumbinary orbits. The curves show most circular paths around Kepler-16 at the orbital distance of Kepler-16b, both in isolation (magenta curve) and with a Jupiter-mass planet orbiting with $e \approx 0$ at 2 AU (blue curve). The difference between these two trajectories (cyan curve; offset for comparison) compares well with data from a satellite orbiting a single star with the mass of Kepler-16 and a Jupiter-mass companion (orange curve). These lower curves show that the most circular path provides a frame of reference for the action of external perturbations, just like a circularly orbiting guiding center in the circumstellar case.

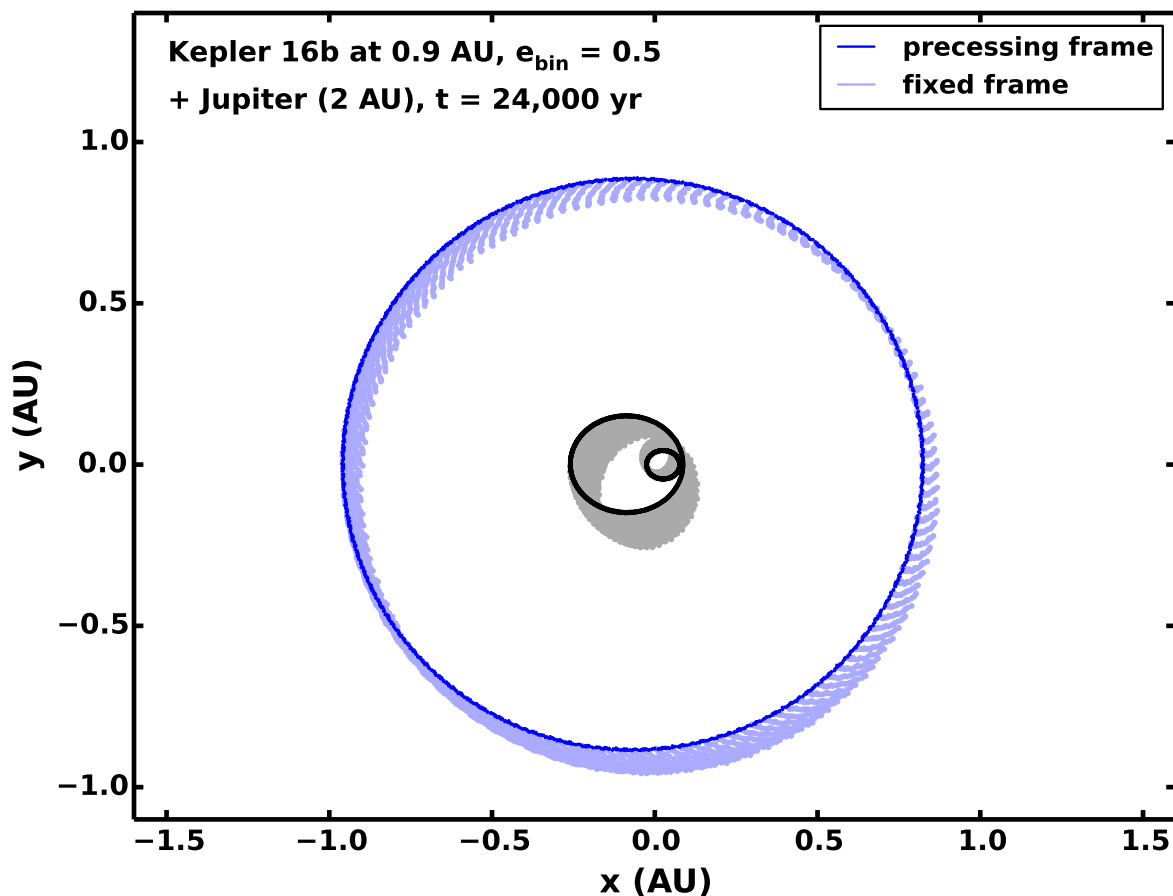


Fig. 6.— Binary precession and circumbinary orbits in a simulation. The outer curves show most circular paths ($a = 0.9$ AU) around a binary like Kepler-16, set with eccentricity of 0.5 (inner curves) and with a Jupiter-mass planet orbiting with $e \approx 0$ at 2 AU. The light-shaded curves show orbits in the inertial reference frame of the system’s center of mass. The duration of the simulation is about a quarter of the precession period; orbits have precessed about 90° (see Equation (49)). The dark-shaded curves are the same orbits represented in a reference frame that precesses with the binary’s periape. The satellite’s forced epicyclic motion evidently precesses at this rate.

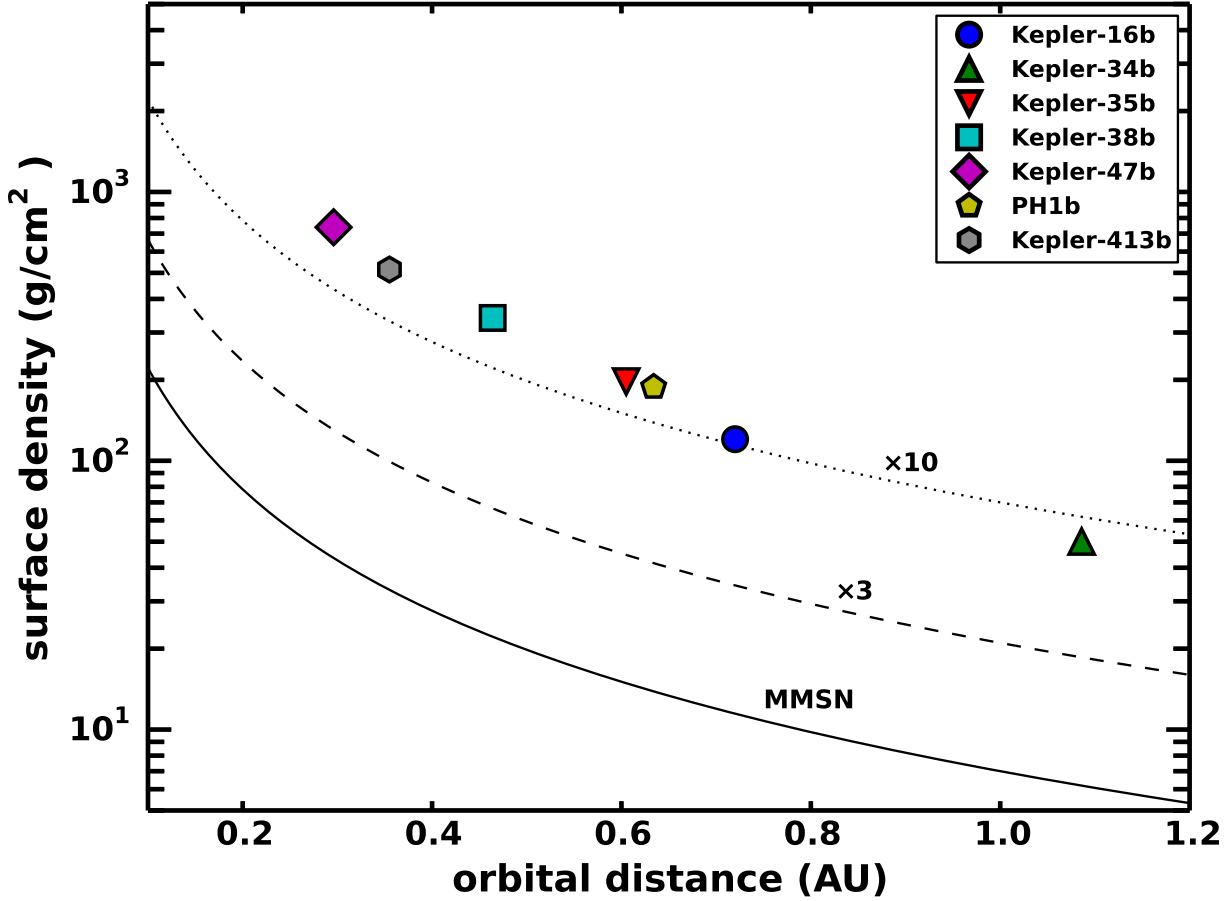


Fig. 7.— The minimum surface density to build the *Kepler* circumbinary planets. Each planet is shown at its orbital distance from the host binary. The value of the surface density (Σ) comes from determining an annular width from which the planet could have accreted mass, based on its escape velocity when it had the mass of a $10 M_{\oplus}$, prior to its acquisition of a gas atmosphere (from Equation (58)). The solid line is the surface density of a Minimum Mass Solar Nebula ($\Sigma = 7(a/1 \text{ AU})^{-1.5} \text{ g/cm}^2$), while the dashed and dotted lines correspond to disks with three and ten times that density (as labeled). Indications from simulations (e.g., Kenyon & Bromley 2006) suggest that the intermediate-mass disk is a realistic starting condition for the Solar nebula.

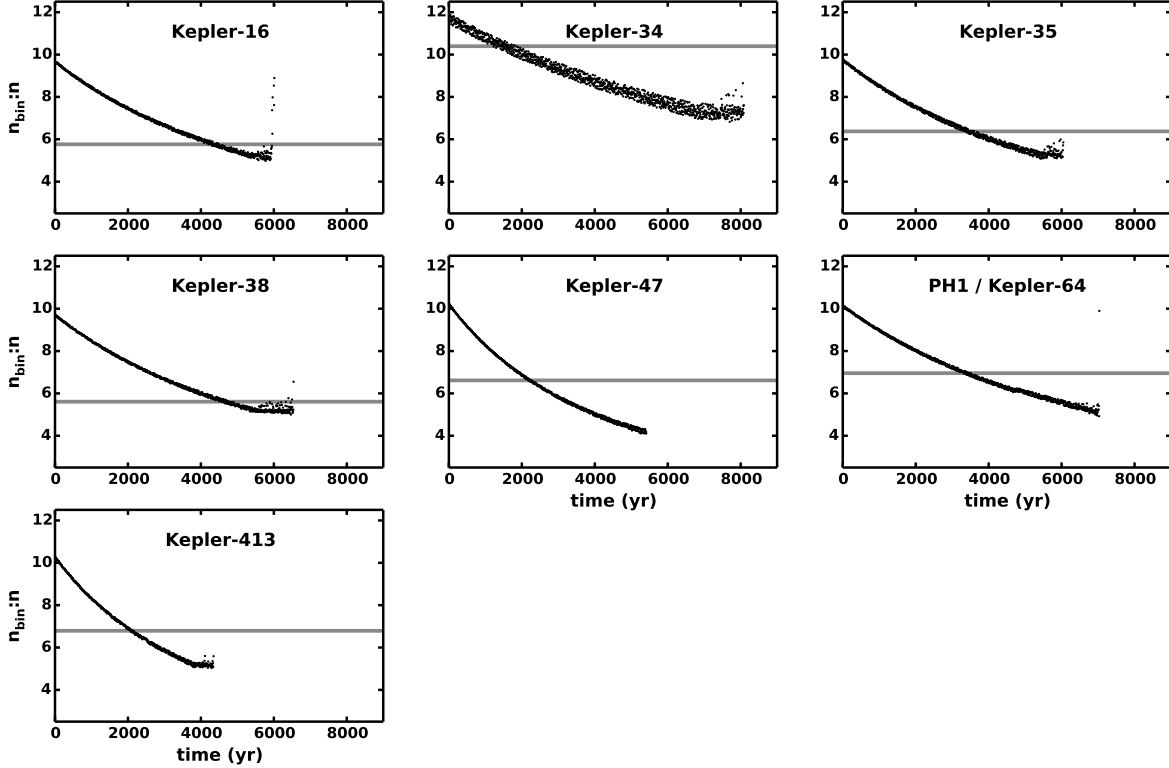


Fig. 8.— Stability of circumbinary orbits. Each panel shows the ratio of orbital frequencies between the central binary and the circumbinary planet. To mimic migration, we smoothly adjust the binary semimajor axis to cover the observed ratio of orbital frequencies (gray line). The end of each curve indicates where the orbit of the planet becomes unstable. For most planets, the 5:1 resonance is disruptive. Kepler-34b, whose binary host has high eccentricity ($e = 0.5$), goes unstable when it hits the 7:1 resonance. The planet around Kepler-47, with the lowest binary eccentricity of the group ($e = 0.023$), is stable down to the 4:1 resonance. Directly migrating the planet by artificially adjusting its semimajor axis gives similar results, except the planet around Kepler-34 remains bound. Here, we choose to gradually expand the binary’s semimajor axis while preserving all other orbital elements. It is mathematically equivalent, and it is more straightforward to adjust the Keplerian orbit of the binary than the non-Keplerian orbit of the planet.